

# 1 Basic chemical compositions combination rules and quantitative criterion of red beds

2

3 Guangjun Cui <sup>1,2</sup>, Jin Liao <sup>2</sup>, Linghua Kong <sup>2</sup>, Cuiying Zhou <sup>2,\*</sup>, Zhen Liu <sup>2,\*</sup>, Lei Yu <sup>2</sup>,

4 Lihai Zhang <sup>3</sup>

5

6 <sup>1</sup> Institute of Estuarine and Coastal Research/Guangdong Provincial Engineering Research Center of  
7 Coasts, Islands and Reefs, School of Ocean Engineering and Technology, Sun Yat-sen University,  
8 Guangzhou 510275, China

9 <sup>2</sup> Guangdong Engineering Research Center for Major Infrastructures Safety, Sun Yat-sen University,  
10 Guangzhou, 510275, China

11 <sup>3</sup> The University of Melbourne, Melbourne VIC 3010, Australia

12 \*Correspondences: [zhoucy@mail.sysu.edu.cn](mailto:zhoucy@mail.sysu.edu.cn) (C. Zhou), [liuzh8@mail.sysu.edu.cn](mailto:liuzh8@mail.sysu.edu.cn) (Z. Liu)

13

## 14 Abstract

15 Red beds belong to slippery formations, and their rapid identification is of great significance for  
16 major scientific and engineering issues such as geological hazard risk assessment and rapid response.  
17 Existing research often identifies red beds from a qualitative or semi quantitative perspective, resulting  
18 in slow recognition speed and inaccurate recognition results, making it difficult to quickly handle  
19 landslide geological disasters. Combined with the correlation between red beds geomorphic  
20 characteristics, mineral compositions, and chemical compositions, this study established a preliminary  
21 identification quantitative criterion based on the basic chemical composition combination rules  
22 ( $\text{SiO}_2+\text{Al}_2\text{O}_3$ ,  $\text{Al}_2\text{O}_3/\text{SiO}_2$ ,  $\text{FeO}+\text{Fe}_2\text{O}_3$ ,  $\text{Fe}_2\text{O}_3/\text{FeO}$ ,  $\text{K}_2\text{O}+\text{Na}_2\text{O}$ ,  $\text{Na}_2\text{O}/\text{K}_2\text{O}$ ,  $\text{CaO}+\text{MgO}$ , and  $\text{MgO}/\text{CaO}$ )  
23 in the red beds. Then, perform principal component analysis on the basic chemical composition  
24 combination rules mentioned above. The results indicate that simultaneously meeting the following  
25 **principal component features** can serve as a rapid quantitative criterion for distinguishing red beds from  
26 other rocks:  $F1=-3.36\sim 23.55$ ,  $F2=-23.00\sim 3.11$ ,  $F3=-10.12\sim 4.88$ ,  $F4=-2.21\sim 4.52$ ,  $F5=-0.97\sim 7.30$ , and  
27  $F=-0.67\sim 1.89$ . By comparing the chemical composition combinations of 15 kinds of rocks collected  
28 from China in this study, it is proven that the quantitative criterion proposed in this study are effective.

29 The study results can be used for rapid identification of red beds, achieving risk assessment and rapid  
30 response of geological disasters such as landslides.

31 **Keywords:** red beds, quantitative criterion, geological disasters, rapid response, chemical compositions

32

### 33 **1. Introduction**

34 Red beds are widely distributed throughout the world (Zhou et al., 2023b; Yan et al., 2019; Chen  
35 et al., 2021). Geological disasters occur frequently in the red beds distribution area, especially landslides,  
36 debris flows, collapses, and underground engineering damage (Chen et al., 2014; Zhou et al., 2023a;  
37 Wang et al., 2022b). According to the characteristics of disasters such as landslides, the red beds belong  
38 to “landslide prone strata”, and the instability of slopes with weak interlayers of the red beds is  
39 particularly evident (Zhang et al., 2015). This is mainly due to the strong hydrophilicity and weak  
40 permeability of the red beds, which are prone to softening and plastic deformation under the action of  
41 water; After absorbing water, the red beds are easy to expand, and after losing water, they are easy to  
42 contract; The weathering resistance of the red beds are weak, they are easy to collapse, and their  
43 compressive and shear strength are low (Zhang et al., 2016; Wu et al., 2018; Wang et al., 2017; Marat  
44 et al., 2022; Zhang et al., 2024). The red beds have different lithology or poor binding force with other  
45 rock strata, which can easily cause differential deformation and lead to rock mass sliding along the  
46 bedding plane (Liu et al., 2020; He et al., 2023; Wang et al., 2024). Therefore, the identification of rock  
47 types, especially the rapid determination of red beds, is of great significance for major scientific and  
48 engineering issues such as risk assessment and rapid response of geological disasters in red beds  
49 distribution area.

50 At present, the studies on red beds identification are mostly carried out from the perspectives of  
51 geomorphic characteristics, mineral compositions, and chemical compositions (Cui et al., 2022; Zhou  
52 et al., 2021). **And, there is a close relationship between these perspectives (Moonjun et al., 2017;  
53 Bankole et al., 2016; Perri et al., 2013). For example, the content of Fe<sub>2</sub>O<sub>3</sub> or hematite in the red beds  
54 is higher than that in the grey beds (Hu et al., 2006).** Among these perspectives, the research of  
55 geomorphic characteristics and mineral compositions mostly adopts qualitative or semi quantitative  
56 methods, and there are many such studies. For example, Rainoldi et al. (2015) identified red beds by

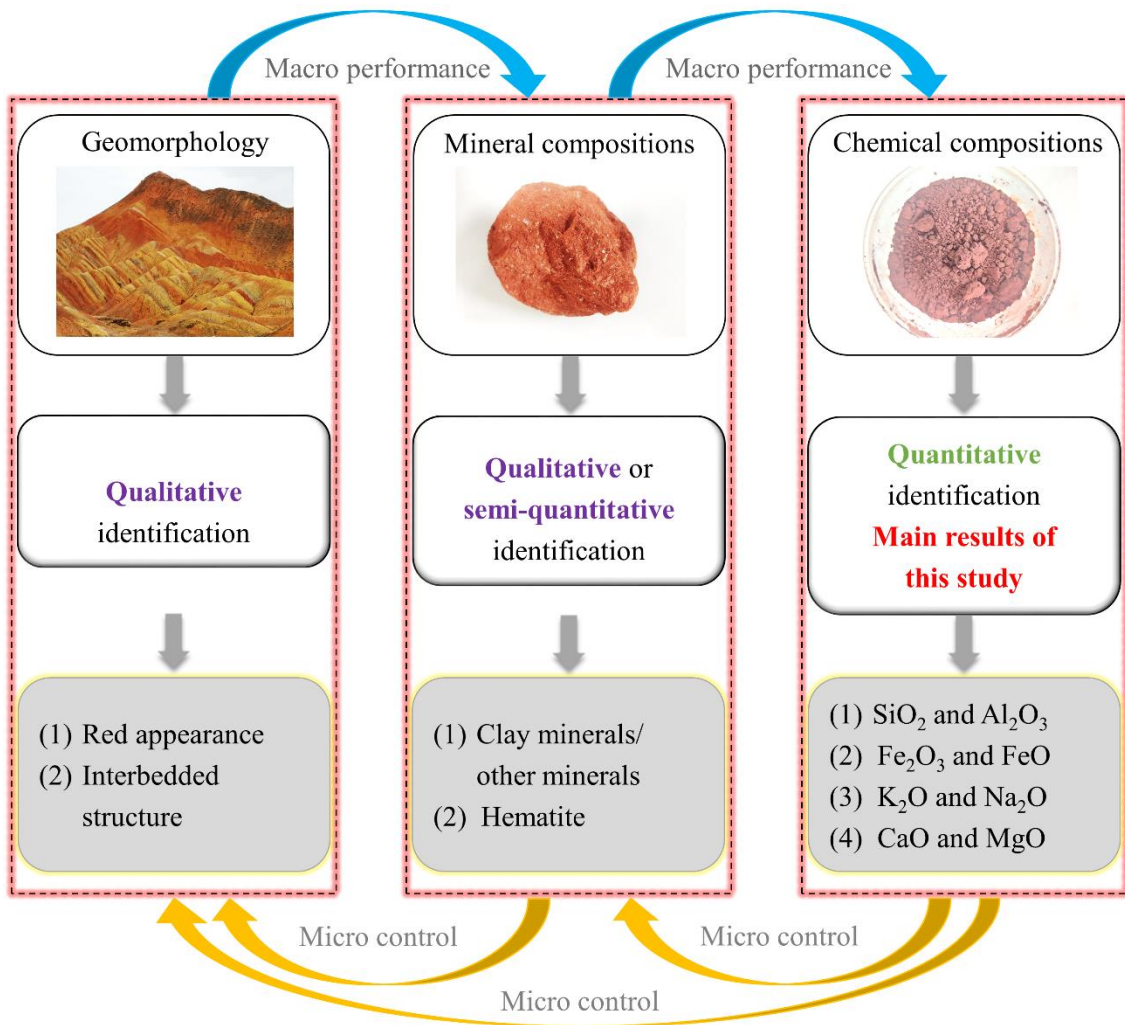
57 studying the color of geomorphic characteristics and hematite in mineral compositions, and studied the  
58 mechanism of red beds bleaching. Uchida et al. (2000) distinguished red sandstone, yellowish brown  
59 sandstone, and green sandstone according to the content of hematite, goethite, biotite, and muscovite in  
60 the mineral compositions, analyzed the characteristics of different rocks and pointedly protected  
61 Angkor monuments. Xue et al. (2023) distinguished red mudstone and red sandstone by quantifying the  
62 clay mineral content in the mineral compositions, in order to analyze the mechanisms and control factors  
63 of summer uplift of high-speed railway cutting. **At this stage, the research on the geomorphology,  
64 mineral color and clay content of the red beds lays the foundation for the identification of the red beds,  
65 but this identification is still vague and needs to be further quantified. Therefore,** some scholars have  
66 conducted quantitative studies on the chemical compositions of red beds. Hong et al. (2009) analyzed  
67 the alteration of clay minerals by studying the changes in the  $\text{SiO}_2/\text{Al}_2\text{O}_3$  ratio in the chemical  
68 compositions of the red beds, thereby obtaining the weathering degree of the red beds. Bankole et al.  
69 (2016) studied the relationship between Fe/Mg ratio,  $\text{Fe}^{3+}/\text{FeT}$  ratio, and Cr/Fe ratio of red beds to  
70 indirectly study the oxygen content of the Paleoproterozoic. Hu et al. (2006) studied the characteristics  
71 of high  $\text{Fe}_2\text{O}_3$  content and low FeO content in the oceanic red beds, and analyzed ancient landslides on  
72 the continental margin from the perspective of petrology. However, these studies do not distinguish  
73 between red beds and other rocks in terms of chemical compositions. The use of portable spectrometers  
74 and drone-borne multi-sensor remote sensing technique can quickly obtain the chemical compositions  
75 of rocks in geological disasters while ensuring safety (Triantafyllou et al., 2021; Kirsch et al., 2018),  
76 making it feasible to use chemical compositions as the standards to distinguish red beds from other  
77 rocks.

78 Therefore, the purpose of this study to develop a quantitative criterion for quickly and accurately  
79 identifying the red beds. This study first collected the data about the geomorphic characteristics, mineral  
80 content, and chemical composition of red beds and other rocks, then compared these data to obtain the  
81 basic characteristics of red beds, and finally summarized and analyzed the red beds identification  
82 criterion and verified the reliability of this criterion.

83

## 84 **2. Methods**

85 Figure 1 shows the methodology used in this study involving the investigation of geomorphic  
 86 characteristics, mineral compositions, and chemical compositions (the perspective of chemical  
 87 compositions is the focus of this study). In this study, data on geomorphological features, mineral  
 88 content and chemical composition of the red beds and other rocks were first collected, then these data  
 89 were compared to derive the basic characteristics of the red beds, and finally the red bed identification  
 90 criteria were summarized and analyzed, and the reliability of the criteria was verified.



91

92 **Figure 1.** Methodology for identifying red beds from geomorphic characteristics, mineral  
 93 compositions, and chemical compositions.

94

95 2.1 Data collection

96

97

The geomorphic characteristics data were collected from the previous studies about landslides, debris flows, and collapses on of red beds, igneous rocks (andesite, basalt, diorite, granite),

98 metamorphic rocks (gneiss, marble), and other sedimentary rocks (arkose, black-shale, breccia,  
99 claystone, dolomite, lignite, limestone, marl, mudstone, siliciclastic, tuff) (e.g., (Zhang et al., 2015; San  
100 et al., 2020; He et al., 2021; Ciftci et al., 2008; Perez-Rey et al., 2019; Anbarasu et al., 2010; Xia et al.,  
101 2019; Gokbulak and Ozcan, 2008; Li et al., 2016; Wang et al., 2022a; Zhang et al., 2017; Underwood  
102 et al., 2016; Kavvadas et al., 2020; Harp et al., 2011; De Montety et al., 2007; Contino et al., 2017; Liu  
103 et al., 2018; Ni et al., 2015; Hale et al., 2021)). The geomorphic characteristics of red beds investigated  
104 in this study involve the evolution process and distribution of red beds on Earth's surface, and the results  
105 were compared with that of other types of rock samples.

106 The mineral compositions of red beds (1,536 groups data) were collected from the previous studies  
107 as shown in Supplementary Table 1 (e.g., (Jian et al., 2009; Liu et al., 2020; Zha et al., 2022; Bai et al.,  
108 2020; Zhang et al., 2021; Zhang et al., 2020; Yao et al., 2016; Li et al., 2023; Marat et al., 2022; Wang  
109 et al., 2017; Chen et al., 2014; Zhang et al., 2016; Li et al., 2015; Li et al., 2013; Wang et al., 2018;  
110 Wang et al., 2014)). These studies used semi quantitative or quantitative methods in XRD technology  
111 to statistically analyze the differences in mineral composition between different red beds (e.g., quartz,  
112 feldspar, mica, hematite, clay minerals, and calcite), as detailed in the aforementioned literatures. This  
113 study mainly focuses on the influence of mineral compositions on geomorphic characteristics,  
114 particularly the layered structure and color of red beds.

115 The chemical compositions of red beds (1536 groups data) with different geological ages and  
116 various lithologies such as conglomerate, sandy conglomerate, sandstone, siltstone, shale and mudstone  
117 were collected from the previous studies as shown in Supplementary Table 2 (e.g., (Uchida et al., 2000;  
118 Xue et al., 2023; Jiang et al., 2022; Yang et al., 2016; Liu et al., 2020; Kong et al., 2018; Zhao et al.,  
119 2005; Gao et al., 2017; Zhang et al., 2008; Liu et al., 2006; Zhu et al., 2003; Liu et al., 2007; Hong et  
120 al., 2009; Wild et al., 2017)). The chemical compositions of igneous rocks, including andesite  
121 (Supplementary Table 3 - 49,203 groups data. Data were downloaded from the GEOROC database  
122 (<https://georoc.mpch-mainz.gwdg.de/georoc/>) on 11 May 2023, using the following parameters: search  
123 = andesite), basalt (Supplementary Table 4 - 80,365 groups data. Data were downloaded from the  
124 GEOROC database on 11 May 2023, using the following parameters: search = basalt), diorite  
125 (Supplementary Table 5 - 4,941 groups data. Data were downloaded from the GEOROC database on

126 11 May 2023, using the following parameters: search = diorite), and granite (Supplementary Table 6 -  
127 17,272 groups data. Data were downloaded from the GEOROC database on 11 May 2023, using the  
128 following parameters: search = granite). The chemical compositions of metamorphic rocks, including  
129 gneiss (Supplementary Table 7 - 24,300 groups data. The data were downloaded from the EarthChem  
130 Portal Database (<http://portal.earthchem.org/>) on 20 April, 2018, using the following parameters:  
131 material = metamorphic and rock name = gneiss) and marble (Supplementary Table 8 - 3,364 groups  
132 data. The data were downloaded from the EarthChem Portal Database on 12 May, 2023, using the  
133 following parameters: material = metamorphic and rock name = marble). The chemical compositions  
134 of other sedimentary rocks, including arkose (Supplementary Table 9 - 682 groups data. The data were  
135 downloaded from the EarthChem Portal Database on 10 May, 2023, using the following parameters:  
136 material = sedimentary and rock name = arkose), black-shale (Supplementary Table 10 - 305 groups  
137 data. The data were downloaded from the EarthChem Portal Database on 10 May, 2023, using the  
138 following parameters: material = sedimentary and rock name = black-shale), breccia (Supplementary  
139 Table 11 - 1,396 groups data. The data were downloaded from the EarthChem Portal Database on 10  
140 May, 2023, using the following parameters: material = sedimentary and rock name = breccia), claystone  
141 (Supplementary Table 12 - 3,790 groups data. The data were downloaded from the EarthChem Portal  
142 Database on 10 May, 2023, using the following parameters: material = sedimentary and rock name =  
143 claystone), dolomite (Supplementary Table 13 - 2,169 groups data. The data were downloaded from the  
144 EarthChem Portal Database on 6 May, 2023, using the following parameters: material = sedimentary  
145 and rock name = dolomite), lignite (Supplementary Table 14 - 3 groups data. The data were downloaded  
146 from the EarthChem Portal Database on 24 April, 2018, using the following parameters: material =  
147 sedimentary and rock name = lignite), limestone (Supplementary Table 15 - 9,104 groups data. The  
148 data were downloaded from the EarthChem Portal Database on 10 May, 2023, using the following  
149 parameters: material = sedimentary and rock name = limestone), marl (Supplementary Table 16 - 142  
150 groups data. The data were downloaded from the EarthChem Portal Database on 10 May, 2023, using  
151 the following parameters: material = sedimentary and rock name = marlstone, marl), mudstone  
152 (Supplementary Table 17 - 6,140 groups data. The data were downloaded from the EarthChem Portal  
153 Database on 10 May, 2023, using the following parameters: material = sedimentary and rock name =

154 mudstone, mud), siliciclastic (Supplementary Table 18 - 26,938 groups data. The data were downloaded  
 155 from the EarthChem Portal Database on 10 May, 2023, using the following parameters: material =  
 156 sedimentary and rock name = siliciclastic), tuff (Supplementary Table 19 - 10,295 groups data. The  
 157 data were downloaded from the EarthChem Portal Database on 6 May, 2023, using the following  
 158 parameters: material = sedimentary and rock name = tuff).

159 Studies have found that rock disasters are related to the content of minerals such as quartz, clay  
 160 minerals, hematite, calcite, dolomite, feldspar, etc., and these mineral contents are also closely related  
 161 to the combination of major elements or oxides (Table 1), for example, SiO<sub>2</sub> and Al<sub>2</sub>O<sub>3</sub> (used to study  
 162 the relative content relationship between quartz and clay minerals) (Hong et al., 2009), Fe<sub>2</sub>O<sub>3</sub> and FeO  
 163 (used to study the high content characteristics of hematite) (Hu et al., 2006), CaO and MgO (used to  
 164 study the content relationship of potassium feldspar, calcite, and dolomite) (Han et al., 2023), Na<sub>2</sub>O and  
 165 K<sub>2</sub>O (Qiao et al., 2017). Therefore, this study on the basic chemical composition combination rules and  
 166 quantitative criterion of the red beds only involves the major elements mentioned above, and does not  
 167 involve the analysis of trace elements or other stable isotopes.

168 **Table 1.** Chemical composition (%) of minerals in red beds from database.

Mineral chemical formulas	SiO <sub>2</sub>	Al <sub>2</sub> O <sub>3</sub>	Fe <sub>2</sub> O <sub>3</sub>	FeO	CaO	MgO	Na <sub>2</sub> O	K <sub>2</sub> O	H <sub>2</sub> O	CO <sub>2</sub>
Quartz (SiO <sub>2</sub> )	100.0									
Potassium feldspar (KAlSi <sub>3</sub> O <sub>8</sub> )	64.7	18.4						16.9		
Sodium feldspar (NaAlSi <sub>3</sub> O <sub>8</sub> )	68.8	19.4					11.8			
Calcium feldspar (CaAl <sub>2</sub> Si <sub>2</sub> O <sub>8</sub> )	43.2	36.7			20.1					
White mica (KAl <sub>2</sub> (AlSi <sub>3</sub> O <sub>10</sub> )(OH,F) <sub>2</sub> )	45.2	38.4						11.8	4.1	
Biotite (KMg <sub>3</sub> [Si <sub>3</sub> AlO <sub>10</sub> ](OH,F) <sub>2</sub> )	43.0	12.2				28.8		11.2	2.2	
Phlogopite (K(Mg,Fe) <sub>3</sub> AlSi <sub>3</sub> O <sub>10</sub> (F,OH) <sub>2</sub> )	41.6	11.8		8.3		23.2	0.5	10.9	3.6	
Hematite (Fe <sub>2</sub> O <sub>3</sub> )			100.0							
Calcite (CaCO <sub>3</sub> )					56.0					44.0
Kaolinite (Al <sub>2</sub> Si <sub>2</sub> O <sub>5</sub> (OH) <sub>4</sub> )	46.6	39.5							14.0	
Illite (K <sub>0.75</sub> (Al <sub>1.75</sub> R)[Si <sub>3.5</sub> Al <sub>0.5</sub> O <sub>10</sub> ](OH) <sub>2</sub> )	54.0	17.0		1.9		3.1		7.3	12.0	
Montmorillonite (Na,Ca) <sub>0.33</sub> (Al,Mg) <sub>2</sub> [Si <sub>4</sub> O <sub>10</sub> ](OH) <sub>2</sub> ·nH <sub>2</sub> O	43.8	18.6			1.0		1.1		36.1	
Chlorite (Y <sub>3</sub> [Z <sub>4</sub> O <sub>10</sub> ](OH) <sub>2</sub> ·Y <sub>3</sub> (OH) <sub>6</sub> )	30.3	17.1		15.1		25.4			12.1	

169 Note: Data collected from <http://webmineral.com/> and <https://www.mindat.org/>.

170

171 Using SPSS PRO online data analysis program and principal component analysis method to compare the

172 chemical components combination rules of red beds, the identification quantitative criterion was studied at a  
173 significance level of  $P < 0.05$ .

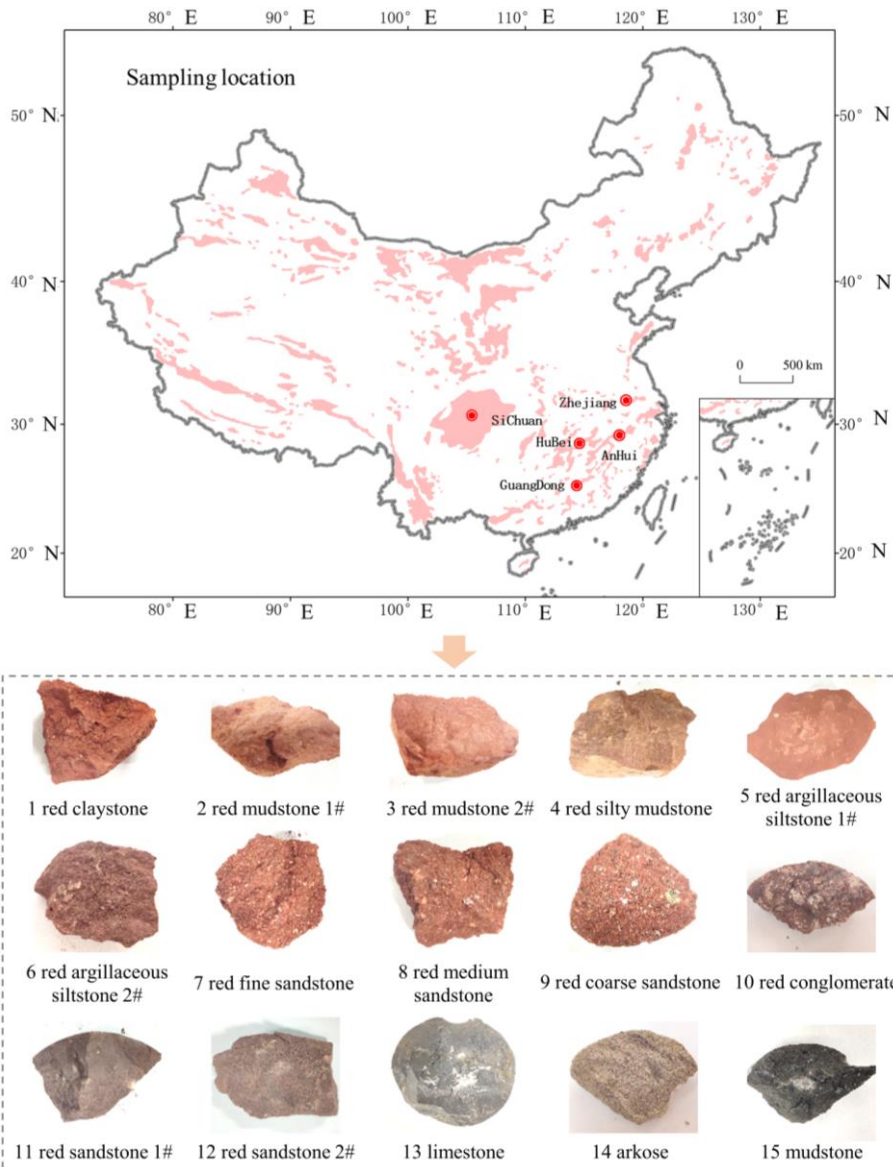
174

## 175 2.2 Criterion verification

176 In order to verify the proposed basic chemical compositions combination rules and quantitative  
177 criterion of red beds, 15 kinds of rocks of known rock types were selected in Guangdong, Sichuan,  
178 Hubei, Zhejiang, and Anhui provinces (Figure 2), including 12 kinds of red beds (red claystone, red  
179 mudstone, red silty mudstone, red argillaceous siltstone, red fine sandstone, red medium sandstone, red  
180 coarse sandstone, red conglomerate, etc.), limestone (1 kind), arkose (1 kind) and mudstone (1 kind).  
181 After on-site sampling, use a hammer to smash the rock block out of the fresh surface. Then, the fresh  
182 surface was analyzed using the YL-P-3LRX Handheld Laser Induced Breakdown Spectroscopy (LIBS,  
183 Figure 3) to check whether these elements conform to the basic chemical compositions combination  
184 rules of red beds proposed by this study. This device can detect elements such as K, Na, Si, Al, Ca, Mg,  
185 Fe, and oxides.

186 The working principle of the LIBS is that a miniature X-ray source provides tube voltage and tube  
187 current, and the light tube emits continuous X-ray spectral lines. The X-rays irradiated on the sample  
188 knock out the inner electrons of the K and L layers of the element atoms, and the holes in the low-  
189 energy layer are filled by high-energy outer electrons (N layer). The high-energy electrons emit excess  
190 energy as X-ray fluorescence ( $K\alpha$ ) with elemental characteristics. Thus, the instrument detects the type  
191 and concentration of elements through the emitted spectral lines. On the instrument analysis interface,  
192 point the detection window towards the rock sample and press the trigger to start and stop the  
193 measurement. After amplification and data collection, the signal is processed to obtain the required test  
194 data.



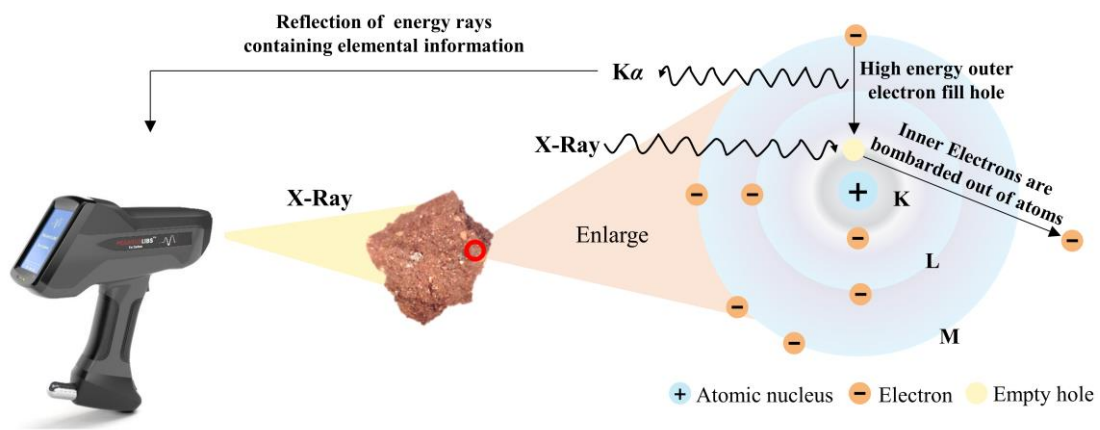


195

196

**Figure 2.** Distribution areas of red beds in China and sampling locations for 15 types of rocks.

197



198

199

**Figure 3.** YL-P-3LRX Handheld Laser Induced Breakdown Spectroscopy and the working principle.

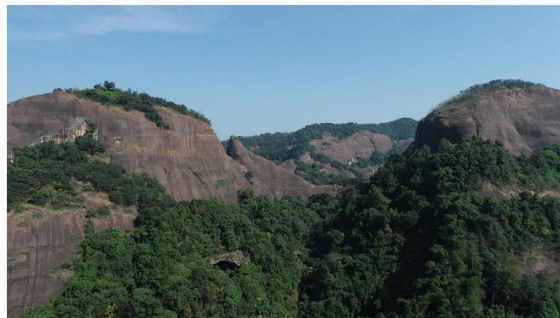
200 **3. Results and discussions**

201 3.1 Geomorphic characteristics of red beds

202 **Geomorphic characteristics of the red beds as shown in Figure 4.** Red beds are sedimentary rocks  
203 of different geological ages (mainly Mesozoic and Cenozoic) with bedding structure typically  
204 consisting of various lithologies such as conglomerate, sandy conglomerate, sandstone, siltstone, shale  
205 and mudstone that are predominantly red in color due to the presence of ferric oxides (Yan et al., 2019).  
206 Owing to differences in depositional environments and influences of late stage geologic processes, the  
207 color of red beds can be brownish-reddish-yellow, brownish-yellow, purplish-red, brownish-red,  
208 grayish-purple and other reddish tints (Yan et al., 2019; Nance, 2015), making it difficult to accurately  
209 describe using the CIELAB color space and/or Munsell color system. Bedding is a common structural  
210 feature of sedimentary rocks representing the changes in the sedimentary environment. The sandstone  
211 is one of the most common types of red beds, with a distinct reddish appearance. **Compared with the**  
212 **obvious layering and red appearance characteristics of red beds,** igneous rocks and metamorphic rocks  
213 do not show the two characteristics of red appearance and bedding at the same time. Basalts are reddish  
214 in appearance but does not have bedding (Cunha et al., 2005). In addition, andesites are mainly light  
215 black and have a columnar structure which is similar to that of basalts (Feizizadeh et al., 2021). Most  
216 of granites are grey or light brown with a significantly different structure compared to red beds (Migon  
217 et al., 2018), while gneisses are generally characterized as a dark and light gneissic structure (Garajeh  
218 et al., 2022). Although the red color appearance and bedding structure can be used as qualitative criteria  
219 for identifying the red beds, the analysis of mineral and chemical compositions is still necessary for  
220 identifying the rocks from quantitative perspective.



221 Red beds Yadan landform



Red beds Danxia landform

222 **Figure 4. Geomorphic characteristics of the red beds.**

223 3.2 Mineral compositions of red beds

224 Table 2 shows the statistical analysis results of mineral compositions of red beds in Supplementary  
 225 Table 1. The common minerals in the red bed are quartz (median value is 40%, the same below), clay  
 226 minerals (35%, including kaolinite, illite, montmorillonite, and chlorite), feldspar (10%, including K-  
 227 feldspar and plagioclase), calcite (10%), mica (7%, including biotite, muscovite and sericite), and  
 228 hematite (3%) according to their content. According to the average value and standard deviation, it can  
 229 be seen that the content range of various minerals has significant dispersion. The ratio of the content of  
 230 clay minerals to other minerals (quartz, feldspar, mica, hematite, and calcite) ranges between 0.11 to  
 231 1.50. The hematite content ranges between 1.5% and 10.0% (percentile=10%~90%), and reddish  
 232 appearance of red beds is due to the abundant hematite content of the rocks. The change in mineral  
 233 compositions of red beds could lead to the change in rock color which is one of the major characteristics  
 234 of red beds. Furthermore, when the red beds encounter water, softening and expansion could happen  
 235 because of the large amount of clay minerals in the rocks, especially the mudstone. The differences in  
 236 mineral compositions of the red beds can also be quantitatively described through their chemical  
 237 composition combination characteristics (Table 1).

238 **Table 2.** The statistical analysis results of mineral compositions of red beds from literature data.

Minerals	Range (per = 0%~100%)	Range (per = 10%~90%)	Median value (per = 50%)	Average value	Standard deviation
Quartz (%)	2.3~94.0	21.0~69.0	40.0	42.6	18.8
Clay minerals (%)	1.0~80.0	7.8~59.0	35.0	34.1	18.6
Feldspar (%)	0.4~71.0	2.3~25.0	10.0	12.6	10.7
Mica (%)	0.1~40.8	3.0~20.0	7.0	9.2	8.2
Hematite (%)	0.4~25.2	1.5~10.0	3.0	5.0	4.4
Calcite (%)	0.7~97.7	3.1~23.5	10.0	12.2	10.0
Clay minerals/ Other minerals	0.01~6.00	0.11~1.50	0.61	0.76	0.66

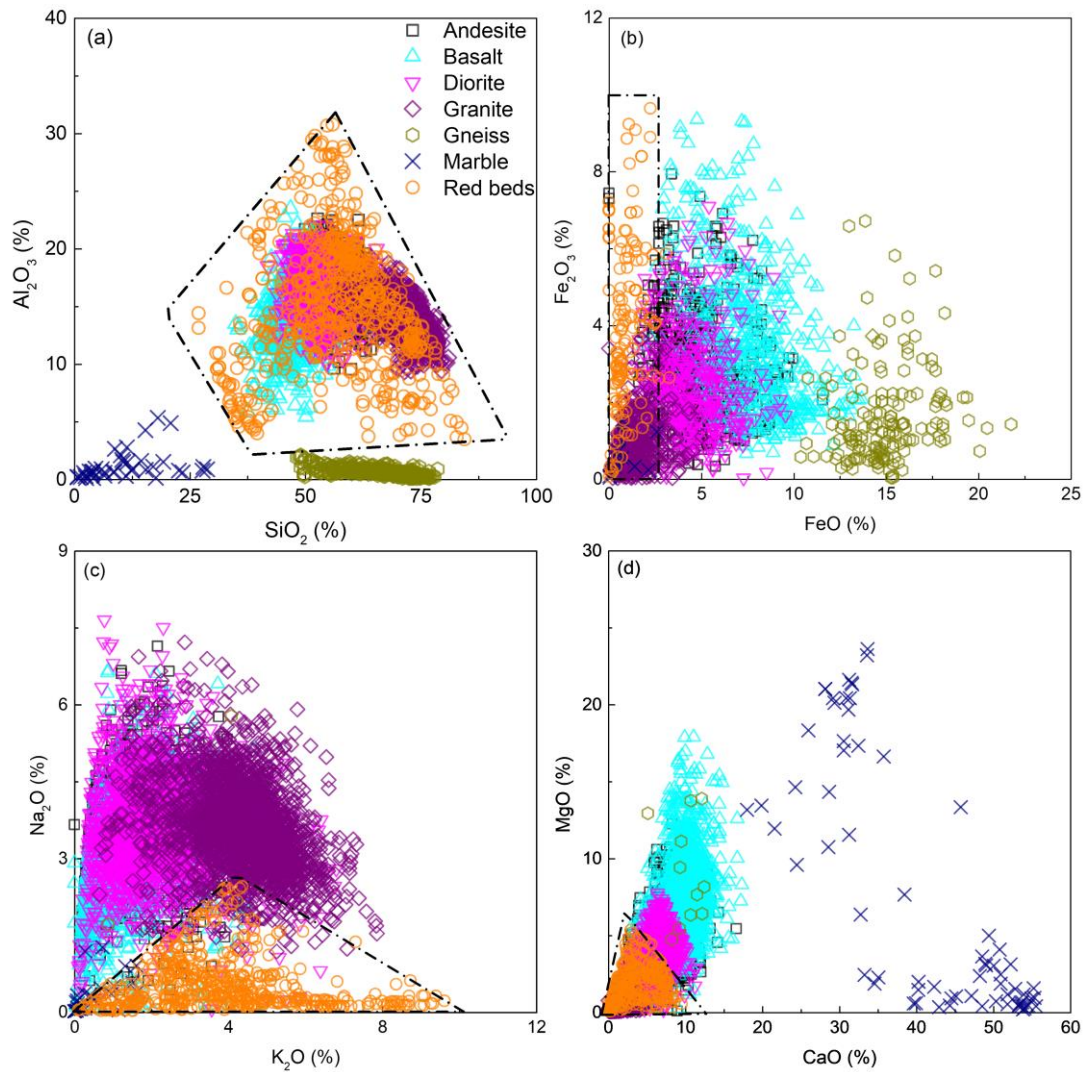
239 Note: per – percentile; Other minerals – quartz, feldspar, mica, hematite, and calcite.

240

241 3.3 Chemical composition characteristics of red beds

242 Figures 5~6 are mainly used to qualitatively analyze the differences in chemical compositions  
 243 between the red beds and other rocks through scatter plots. The area surrounded by black dashed lines  
 244 is the area where the red beds data points are located. To better distinguish various rock data points, the  
 245 distribution areas of various rock data are shown on the right side of the figure, and the corresponding

246 colored dashed ellipses are used to indicate the distribution areas in the dataset. Figure 5 shows the  
 247 comparison of SiO<sub>2</sub> and Al<sub>2</sub>O<sub>3</sub>, FeO and Fe<sub>2</sub>O<sub>3</sub>, K<sub>2</sub>O and Na<sub>2</sub>O, CaO and MgO contents in red beds,  
 248 igneous rocks, and metamorphic rocks, respectively. Figure 6 shows the comparison of SiO<sub>2</sub> and Al<sub>2</sub>O<sub>3</sub>,  
 249 FeO and Fe<sub>2</sub>O<sub>3</sub>, K<sub>2</sub>O and Na<sub>2</sub>O, CaO and MgO contents in red beds and other sedimentary rocks  
 250 respectively.



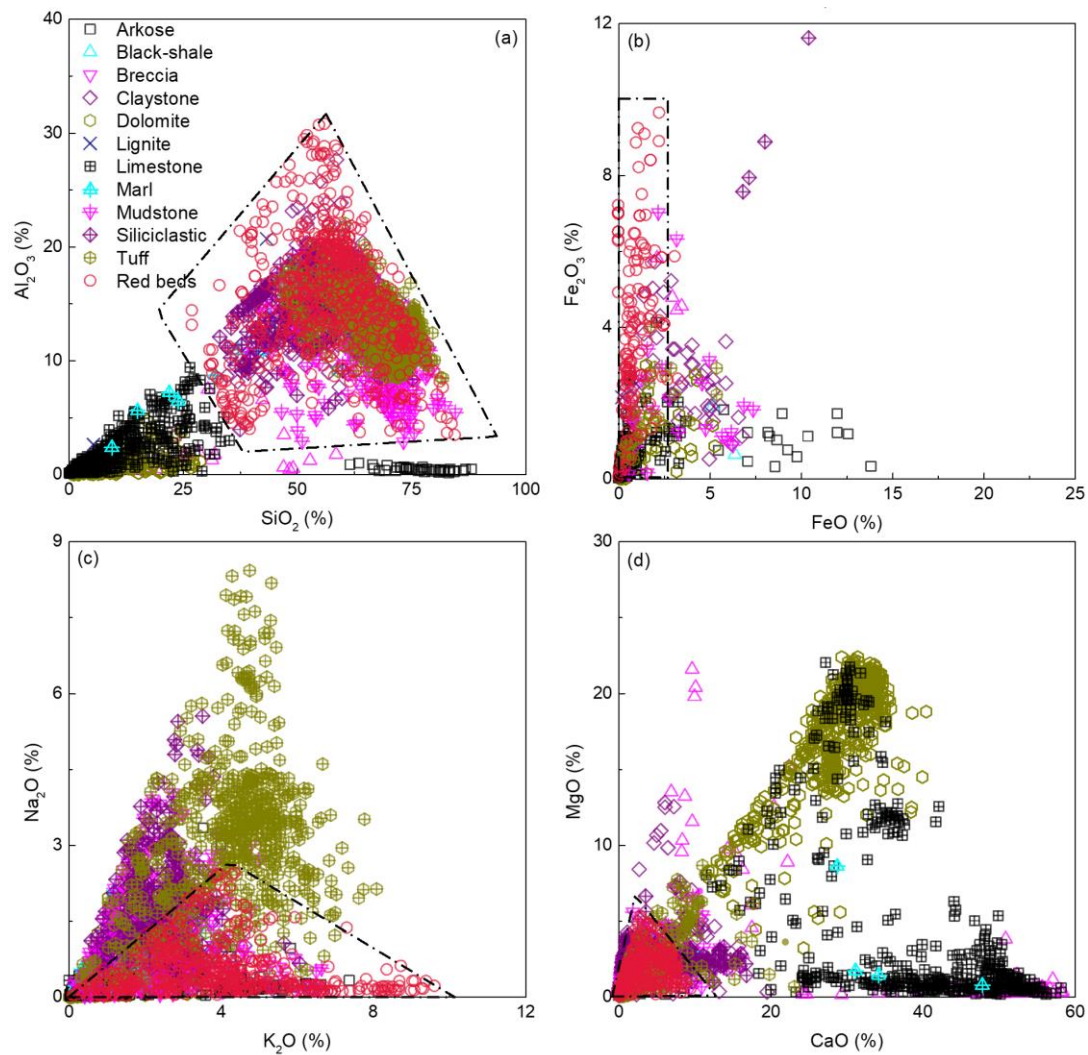
251

252 **Figure 5.** Comparison of (a) SiO<sub>2</sub> and Al<sub>2</sub>O<sub>3</sub>, (b) FeO and Fe<sub>2</sub>O<sub>3</sub>, (c) K<sub>2</sub>O and Na<sub>2</sub>O, (d) CaO and

253 MgO contents in red beds, igneous rock, and metamorphic rocks, respectively. (Note: Icons of the

254 same color in the figure have the same meanings)





255

256 **Figure 6.** Comparison of (a) SiO<sub>2</sub> and Al<sub>2</sub>O<sub>3</sub>, (b) FeO and Fe<sub>2</sub>O<sub>3</sub>, (c) K<sub>2</sub>O and Na<sub>2</sub>O, (d) CaO and MgO  
 257 contents in red beds and other sedimentary rocks respectively. (Note: Icons of the same color in the figure  
 258 have the same meanings)

259

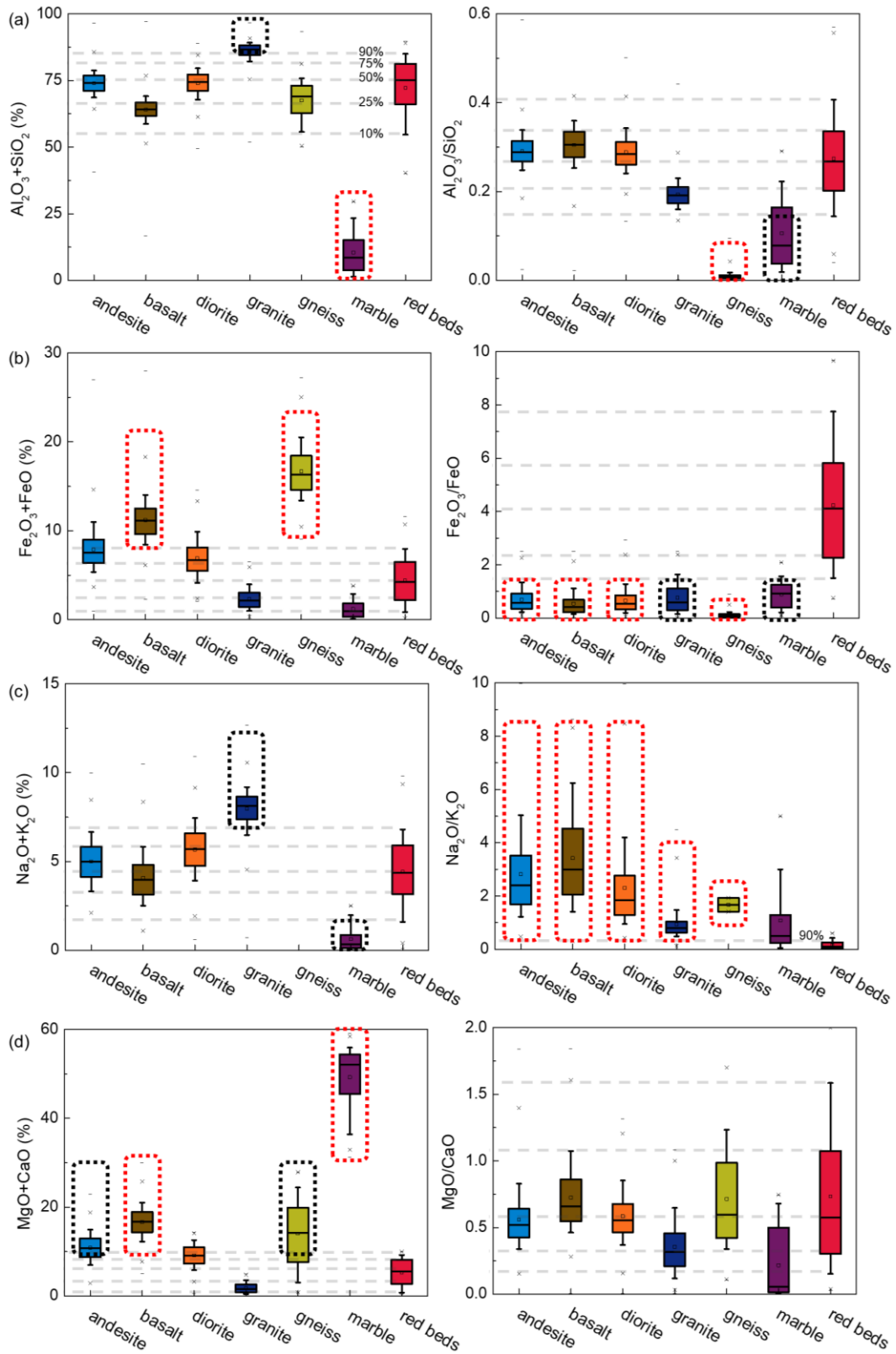
260 The content of SiO<sub>2</sub> in the red beds is about 30%~80%, Al<sub>2</sub>O<sub>3</sub> is about 8%~30%, Fe<sub>2</sub>O<sub>3</sub> is about  
 261 0%~10%, FeO is about 0%~3%, K<sub>2</sub>O is about 0%~10%, Na<sub>2</sub>O is about 0%~2.5%, CaO is about  
 262 0%~10%, and MgO is about 0%~5%. Compared with igneous rocks, metamorphic rocks, and other  
 263 sedimentary rocks, the content of each chemical composition of the red beds has three relationships  
 264 with the content of corresponding chemical composition of other rocks: inclusion relationship (the data  
 265 distribution range of one rock completely covers and is larger than the data range of the other rock),  
 266 intersection relationship (the data distribution range of one rock intersects with the data distribution  
 267 range of another rock), and mutual difference relationship (the data distribution range of one rock does

268 not intersect at all with the data distribution range of another rock). The distribution range of  $\text{SiO}_2$  and  
269  $\text{Al}_2\text{O}_3$  content in the red beds includes the distribution range of  $\text{SiO}_2$  and  $\text{Al}_2\text{O}_3$  content in 9 types of  
270 rocks, namely andesite, basalt, diorite, granite, black shale, claystone, mudstone, siliciclastic, and tuff.  
271 The distribution range of  $\text{SiO}_2$  and  $\text{Al}_2\text{O}_3$  content in the red beds intersects with that in breccia, lignite,  
272 and marl. The distribution range of  $\text{SiO}_2$  and  $\text{Al}_2\text{O}_3$  content in gneiss, marble, arkose, dolomite, and  
273 limestone is different from that in the red beds. The distribution range of  $\text{Fe}_2\text{O}_3$  and FeO content in the  
274 red beds includes the distribution range of  $\text{Fe}_2\text{O}_3$  and FeO content in granite, marble, and lignite. The  
275 distribution range of  $\text{Fe}_2\text{O}_3$  and FeO content in the red beds intersects with that in 8 kinds of rocks,  
276 namely, andesite, basalt, diorite, breccia, claystone, dolomite, limestone, and mudstone. The  
277 distribution range of  $\text{Fe}_2\text{O}_3$  and FeO content in gneiss, arkose, black shale, siliciclastic, and tuff is  
278 different from that in the red beds. The distribution range of  $\text{K}_2\text{O}$  and  $\text{Na}_2\text{O}$  content in the red beds  
279 includes the distribution range of  $\text{K}_2\text{O}$  and  $\text{Na}_2\text{O}$  content in lignite. The distribution range of  $\text{K}_2\text{O}$  and  
280  $\text{Na}_2\text{O}$  content in the red beds intersects with that in 15 kinds of rocks, including andesite, basalt, diorite,  
281 granite, marble, arkose, black shale, breccia, claystone, dolomite, limestone, marl, mudstone,  
282 siliciclastic, and tuff. The distribution range of  $\text{K}_2\text{O}$  and  $\text{Na}_2\text{O}$  content in gneiss is different from that in  
283 the red beds. The distribution range of CaO and MgO content in the red beds includes the distribution  
284 range of CaO and MgO content in granite, black shale, and lignite. The distribution range of CaO and  
285 MgO content in the red beds intersects with that in 13 types of rocks, including andesite, basalt, diorite,  
286 gneiss, arkose, breccia, claystone, dolomite, limestone, marl, mudstone, siliciclastic, and tuff. The  
287 distribution range of CaO and MgO content in marble is different from that in the red beds. Therefore,  
288 from a qualitative perspective, it can be seen that the red beds differ in chemical composition from 8  
289 kinds of rocks, including gneiss, marble, arkose, dolomite, limestone, black-shale, siliciclastic, and tuff,  
290 and also intersects with other rocks to varying degrees. But this is not enough as a criterion to determine  
291 the difference between red beds and other rocks.

292        Figures 7~8 mainly analyze the differences in chemical compositions between red beds and other  
293 rocks through further data statistics and box plots of the scatter plots mentioned above, and propose  
294 quantitative identification criterion for the red beds chemical compositions combination. The red dashed  
295 box in the figure represents rocks that differ from the red beds data, while the black dashed box

296 represents rocks that intersect less than 25% with the red beds data. The data collected in section 2.1  
297 comes from published papers or databases, and its accuracy and robustness have been explained in  
298 relevant literature. In order to ensure the exclusion of outliers in the box plots mentioned above during  
299 the analysis of this study. The horizontal gray dashes corresponding to the red beds box chart represent  
300 10% percentile (the same below), lower quartile (25% percentile), median (50% percentile), upper  
301 quartile (75% percentile), and 90% percentile in the red beds data from bottom to top. Figure 7 shows  
302 the chemical compositions combination comparison of  $\text{SiO}_2+\text{Al}_2\text{O}_3$  (total content, the same below) and  
303  $\text{Al}_2\text{O}_3/\text{SiO}_2$  (content ratio, the same below),  $\text{FeO}+\text{Fe}_2\text{O}_3$  and  $\text{Fe}_2\text{O}_3/\text{FeO}$ ,  $\text{K}_2\text{O}+\text{Na}_2\text{O}$  and  $\text{Na}_2\text{O}/\text{K}_2\text{O}$ ,  
304  $\text{CaO}+\text{MgO}$  and  $\text{MgO}/\text{CaO}$  in red beds, igneous rock, and metamorphic rocks, respectively. Figure 8  
305 respectively shows the chemical compositions combination comparison of  $\text{SiO}_2+\text{Al}_2\text{O}_3$  and  $\text{Al}_2\text{O}_3/\text{SiO}_2$ ,  
306  $\text{FeO}+\text{Fe}_2\text{O}_3$  and  $\text{Fe}_2\text{O}_3/\text{FeO}$ ,  $\text{K}_2\text{O}+\text{Na}_2\text{O}$  and  $\text{Na}_2\text{O}/\text{K}_2\text{O}$ ,  $\text{CaO}+\text{MgO}$  and  $\text{MgO}/\text{CaO}$  in red beds and  
307 other sedimentary rocks.

308 The  $\text{SiO}_2+\text{Al}_2\text{O}_3$  content in the red beds is 54.7%~85.0% (10%~90% percentile, the same below),  
309 the  $\text{Al}_2\text{O}_3/\text{SiO}_2$  ratio is 0.14~0.41, the  $\text{FeO}+\text{Fe}_2\text{O}_3$  content is 0.9%~7.9%, the  $\text{Fe}_2\text{O}_3/\text{FeO}$  ratio is  
310 1.52~7.70, the  $\text{K}_2\text{O}+\text{Na}_2\text{O}$  content is 1.6%~6.8%, the  $\text{Na}_2\text{O}/\text{K}_2\text{O}$  ratio is 0.02~0.43, the  $\text{CaO}+\text{MgO}$   
311 content is 0.8%~9.2%, and the  $\text{MgO}/\text{CaO}$  ratio is 0.16~1.57. By comparing the content of  $\text{SiO}_2+\text{Al}_2\text{O}_3$ ,  
312 the red beds are distinct or have small intersections (less than 25%, the same below) with granite, marble,  
313 dolomite, lignite, limestone, and marl. By comparing the  $\text{Al}_2\text{O}_3/\text{SiO}_2$  ratio, it is found that the red beds  
314 are distinct or have small intersections with gneiss, marble, arkose, and lignite. By comparing the  
315 content of  $\text{FeO}+\text{Fe}_2\text{O}_3$ , it is found that the red beds are distinct or have small intersections with basalt,  
316 gneiss, arkose, and siliciclastic. By comparing the  $\text{Fe}_2\text{O}_3/\text{FeO}$  ratio, it is found that the red beds are  
317 distinct or have small intersections with andesite, basalt, diorite, granite, gneiss, marble, arkose, black  
318 shale, dolomite, mudstone, siliclastic, and tuff. Through the comparison of  $\text{K}_2\text{O}+\text{Na}_2\text{O}$  content, the red  
319 beds are distinct or have small intersections with granite, marble, breccia, dolomite, and limestone. By  
320 comparing the  $\text{Na}_2\text{O}/\text{K}_2\text{O}$  ratio, the red beds are distinct or have small intersections with andesite, basalt,  
321 diorite, gneiss, lignite, siliciclastic, and tuff. Through the comparison of  $\text{CaO}+\text{MgO}$  content, the red  
322 beds are distinct or have small intersections with andesite, basalt, gneiss, marble, breccia, dolomite,  
323 limestone, and marl. By comparing the  $\text{MgO}/\text{CaO}$  ratio, it is difficult to distinguish the red beds from

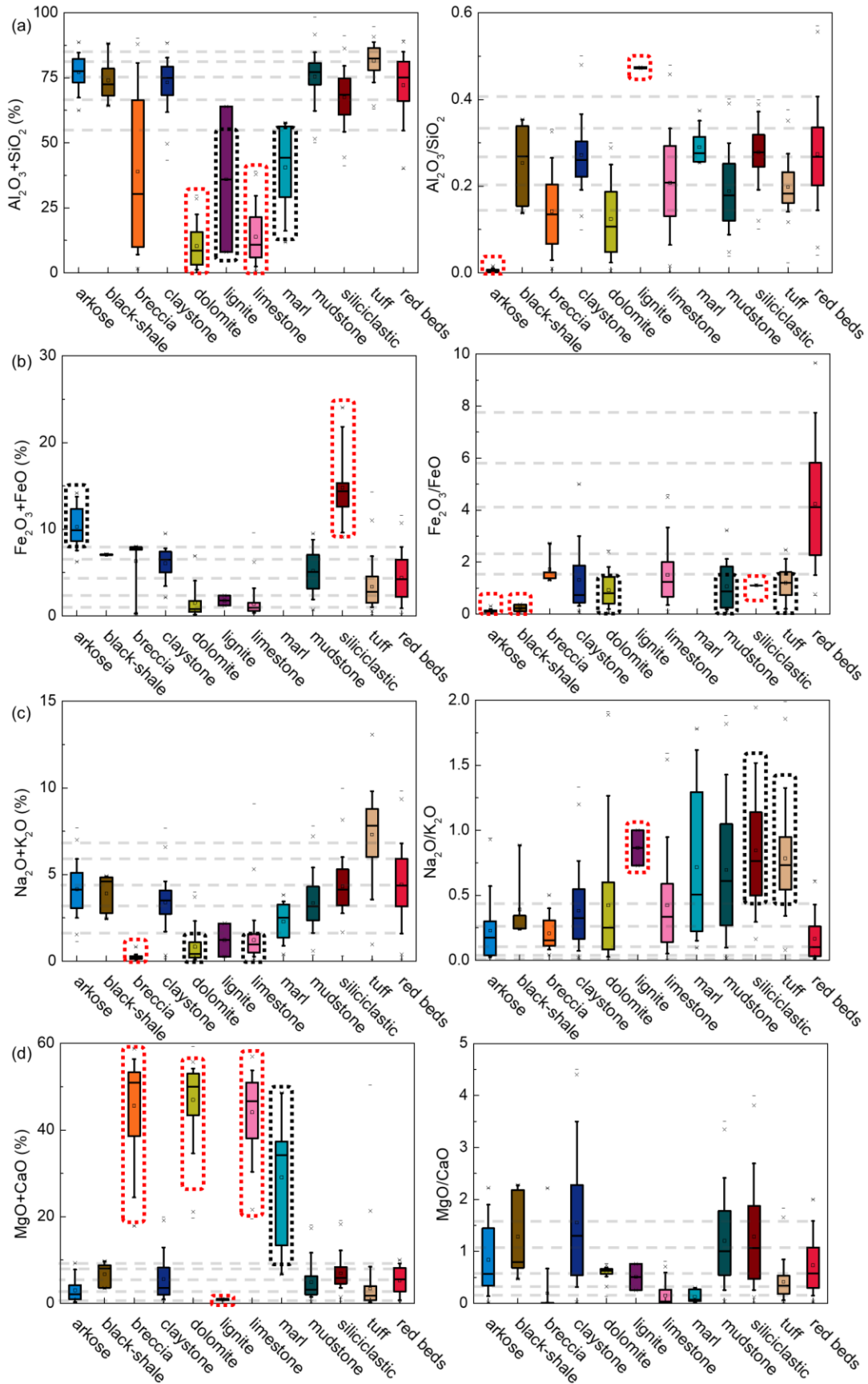


325

326 **Figure 7.** Chemical compositions comparison of (a)  $SiO_2 + Al_2O_3$ ,  $Al_2O_3/SiO_2$ , (b)  $FeO + Fe_2O_3$ ,  $Fe_2O_3/FeO$ ,

327 (c)  $K_2O + Na_2O$ ,  $Na_2O/K_2O$ , (d)  $CaO + MgO$ ,  $MgO/CaO$  in red beds, igneous rock, and metamorphic rocks.





328

329 **Figure 8.** Chemical compositions comparison of (a)  $SiO_2 + Al_2O_3$ ,  $Al_2O_3/SiO_2$ , (b)  $FeO + Fe_2O_3$ ,  $Fe_2O_3/FeO$ ,

330 (c)  $K_2O + Na_2O$ ,  $Na_2O/K_2O$ , (d)  $CaO + MgO$ ,  $MgO/CaO$  in red beds and other sedimentary rocks.

331 In summary, there are differences in chemical compositions between red beds and other rocks.  
 332 Simultaneously meeting the following chemical compositions combinations as a preliminary  
 333 quantitative criterion to distinguish red beds with different geological ages and various lithologies from  
 334 other rocks:  $\text{SiO}_2+\text{Al}_2\text{O}_3 \approx 50.7\%\sim 85.0\%$ ,  $\text{Al}_2\text{O}_3/\text{SiO}_2 \approx 0.14\sim 0.41$ ,  $\text{FeO}+\text{Fe}_2\text{O}_3 \approx 0.9\%\sim 7.9\%$ ,  
 335  $\text{Fe}_2\text{O}_3/\text{FeO} \approx 1.52\sim 7.70$ ,  $\text{K}_2\text{O}+\text{Na}_2\text{O} \approx 1.6\%\sim 6.8\%$ ,  $\text{Na}_2\text{O}/\text{K}_2\text{O} \approx 0.02\sim 0.43$ ,  
 336  $\text{CaO}+\text{MgO} \approx 0.8\%\sim 9.2\%$ , and  $\text{MgO}/\text{CaO} \approx 0.39\sim 1.08$ .

337

### 338 3.4 Principal component analysis and quantitative criterion for red beds identification

339 Based on the preliminary quantitative criterion for identifying the red beds mentioned above, this  
 340 section presents PCA statistical analysis (dimensionality reduction) of the  $\text{SiO}_2+\text{Al}_2\text{O}_3$ ,  $\text{Al}_2\text{O}_3/\text{SiO}_2$ ,  
 341  $\text{FeO}+\text{Fe}_2\text{O}_3$ ,  $\text{Fe}_2\text{O}_3/\text{FeO}$ ,  $\text{K}_2\text{O}+\text{Na}_2\text{O}$ ,  $\text{Na}_2\text{O}/\text{K}_2\text{O}$ ,  $\text{CaO}+\text{MgO}$ , and  $\text{MgO}/\text{CaO}$  of red beds in Figures 7  
 342 and 8. The result is significant with  $P<0.05$  (Table 3), rejecting the null hypothesis. There is correlation  
 343 between the variables, and principal component analysis is effective. It can be seen that the cumulative  
 344 variance interpretation rate of the first five principal components reaches 94.788% (generally greater  
 345 than 90% is sufficient), indicating that using the first five principal components can be well used for  
 346 red beds recognition.

347 **Table 3.** Variance explanation.

Components	Characteristic roots	Variance interpretation rate (%)	Cumulative variance interpretation rate (%)
1	2.700	33.754	33.754
2	2.249	28.112	61.866
3	1.169	14.613	76.479
4	0.882	11.023	87.503
5	0.583	7.285	94.788
6	0.263	3.293	98.081
7	0.131	1.638	99.72
8	0.022	0.280	100.00

348

349 According to the component matrix (Table 4) obtained during the PCA analysis process, the  
 350 calculation equations for 5 principal components  $F1\sim F5$  (Equations 1-5) and the calculation formula  
 351 for the overall principal components  $F$  (Equation 6) can be obtained.

352

353 **Table 4.** Principal component matrix.

Chemical composition combinations	Principal component 1	Principal component 2	Principal component 3	Principal component 4	Principal component 5
SiO <sub>2</sub> +Al <sub>2</sub> O <sub>3</sub>	0.274	-0.281	-0.115	-0.014	-0.009
Al <sub>2</sub> O <sub>3</sub> /SiO <sub>2</sub>	0.085	0.356	0.283	-0.199	-0.352
FeO+Fe <sub>2</sub> O <sub>3</sub>	-0.103	0.334	-0.071	0.449	0.702
Fe <sub>2</sub> O <sub>3</sub> /FeO	0.194	0.038	0.268	0.827	-0.449
K <sub>2</sub> O+Na <sub>2</sub> O	0.213	0.046	0.609	-0.336	0.16
Na <sub>2</sub> O/K <sub>2</sub> O	-0.092	-0.288	0.452	0.179	0.71
CaO+MgO	-0.331	0.05	0.289	-0.153	-0.195
MgO/CaO	0.276	0.196	-0.162	-0.203	0.575

354

355 
$$F1 = 0.274 \times (\text{SiO}_2 + \text{Al}_2\text{O}_3) + 0.085 \times \left(\frac{\text{Al}_2\text{O}_3}{\text{SiO}_2}\right) - 0.103 \times (\text{FeO} + \text{Fe}_2\text{O}_3) + 0.194 \times \left(\frac{\text{Fe}_2\text{O}_3}{\text{FeO}}\right)$$

356 
$$+ 0.213 \times (\text{K}_2\text{O} + \text{Na}_2\text{O}) - 0.092 \times \left(\frac{\text{Na}_2\text{O}}{\text{K}_2\text{O}}\right) - 0.331 \times (\text{CaO} + \text{MgO}) + 0.276 \times \left(\frac{\text{MgO}}{\text{CaO}}\right) \quad (1)$$

357 
$$F2 = -0.281 \times (\text{SiO}_2 + \text{Al}_2\text{O}_3) + 0.356 \times \left(\frac{\text{Al}_2\text{O}_3}{\text{SiO}_2}\right) + 0.334 \times (\text{FeO} + \text{Fe}_2\text{O}_3) + 0.038 \times \left(\frac{\text{Fe}_2\text{O}_3}{\text{FeO}}\right)$$

358 
$$+ 0.046 \times (\text{K}_2\text{O} + \text{Na}_2\text{O}) - 0.288 \times \left(\frac{\text{Na}_2\text{O}}{\text{K}_2\text{O}}\right) + 0.05 \times (\text{CaO} + \text{MgO}) + 0.196 \times \left(\frac{\text{MgO}}{\text{CaO}}\right) \quad (2)$$

359 
$$F3 = -0.115 \times (\text{SiO}_2 + \text{Al}_2\text{O}_3) + 0.283 \times \left(\frac{\text{Al}_2\text{O}_3}{\text{SiO}_2}\right) - 0.071 \times (\text{FeO} + \text{Fe}_2\text{O}_3) + 0.268 \times \left(\frac{\text{Fe}_2\text{O}_3}{\text{FeO}}\right)$$

360 
$$+ 0.609 \times (\text{K}_2\text{O} + \text{Na}_2\text{O}) + 0.452 \times \left(\frac{\text{Na}_2\text{O}}{\text{K}_2\text{O}}\right) + 0.289 \times (\text{CaO} + \text{MgO}) - 0.162 \times \left(\frac{\text{MgO}}{\text{CaO}}\right) \quad (3)$$

361 
$$F4 = -0.014 \times (\text{SiO}_2 + \text{Al}_2\text{O}_3) - 0.199 \times \left(\frac{\text{Al}_2\text{O}_3}{\text{SiO}_2}\right) + 0.449 \times (\text{FeO} + \text{Fe}_2\text{O}_3) + 0.827 \times \left(\frac{\text{Fe}_2\text{O}_3}{\text{FeO}}\right)$$

362 
$$- 0.336 \times (\text{K}_2\text{O} + \text{Na}_2\text{O}) + 0.179 \times \left(\frac{\text{Na}_2\text{O}}{\text{K}_2\text{O}}\right) - 0.153 \times (\text{CaO} + \text{MgO}) - 0.203 \times \left(\frac{\text{MgO}}{\text{CaO}}\right) \quad (4)$$

363 
$$F5 = -0.009 \times (\text{SiO}_2 + \text{Al}_2\text{O}_3) - 0.352 \times \left(\frac{\text{Al}_2\text{O}_3}{\text{SiO}_2}\right) + 0.702 \times (\text{FeO} + \text{Fe}_2\text{O}_3) - 0.449 \times \left(\frac{\text{Fe}_2\text{O}_3}{\text{FeO}}\right)$$

364 
$$+ 0.16 \times (\text{K}_2\text{O} + \text{Na}_2\text{O}) + 0.71 \times \left(\frac{\text{Na}_2\text{O}}{\text{K}_2\text{O}}\right) - 0.195 \times (\text{CaO} + \text{MgO}) + 0.575 \times \left(\frac{\text{MgO}}{\text{CaO}}\right) \quad (5)$$

365 
$$F = (0.338/0.948) \times F1 + (0.281/0.948) \times F2 + (0.146/0.948) \times F3 + (0.11/0.948) \times F4 + (0.073/0.948) \times F5 \quad (6)$$

366

367 Substituting the relevant data of the red beds in Figures 7 and 8 into Equations 1~6 can calculate

368 the quantitative criterion for the red beds:  $F1=-3.36\sim23.55$ ,  $F2=-23.00\sim3.11$ ,  $F3=-10.12\sim4.88$ ,  $F4=-$

369  $2.21\sim4.52$ ,  $F5=-0.97\sim7.30$ , and  $F = -0.67\sim1.89$ .

370

### 371 3.5 Red beds identification quantization criterion verification

372 The chemical composition combinations of the 15 selected rocks in this study are shown in Table  
373 5. Study has found that, The rapid detection of  $\text{Fe}^{2+}$  and  $\text{Fe}^{3+}$  is very difficult (Chen et al., 2019) and  
374 exceeds the detection range of handheld laser-induced breakdown spectroscopy in this manuscript and  
375 similar devices. But this factor does not affect the reliability of the quantification criterion for red beds  
376 recognition.  $F1\sim F5$  and  $F$  are considered as 6 evaluation indicators, and there are a total of 72 ( $6 \times 12$ )  
377 evaluation indicators for the 12 types of red beds. Among them, 3 evaluation indicators exceed the  
378 scope of the quantification criterion for red beds identification ( $F4$  of numbered 7, 9, and 11 red beds  
379 with green background in Table 5 is less than the quantification criterion), indicating that the reliability  
380 of detecting these 12 types of rocks belonging to the red beds is as high as 95.8%. And for 3 non red  
381 beds rocks (limestone, arkose, and mudstone), there are a total of 18 evaluation indicators, of which 13  
382 exceed the scope of the quantification criterion for red beds identification (indicated by blue  
383 background), indicating a high reliability of 72.2% in detecting these three types of rocks that do not  
384 belong to the red beds. Therefore, this study proposes a quantitative criterion for red beds recognition  
385 with high reliability. In the future, if there are new devices that can quickly detect  $\text{Fe}^{2+}$  and  $\text{Fe}^{3+}$ , the  
386 recognition efficiency of the red beds recognition quantification criterion in this study will be higher.

387

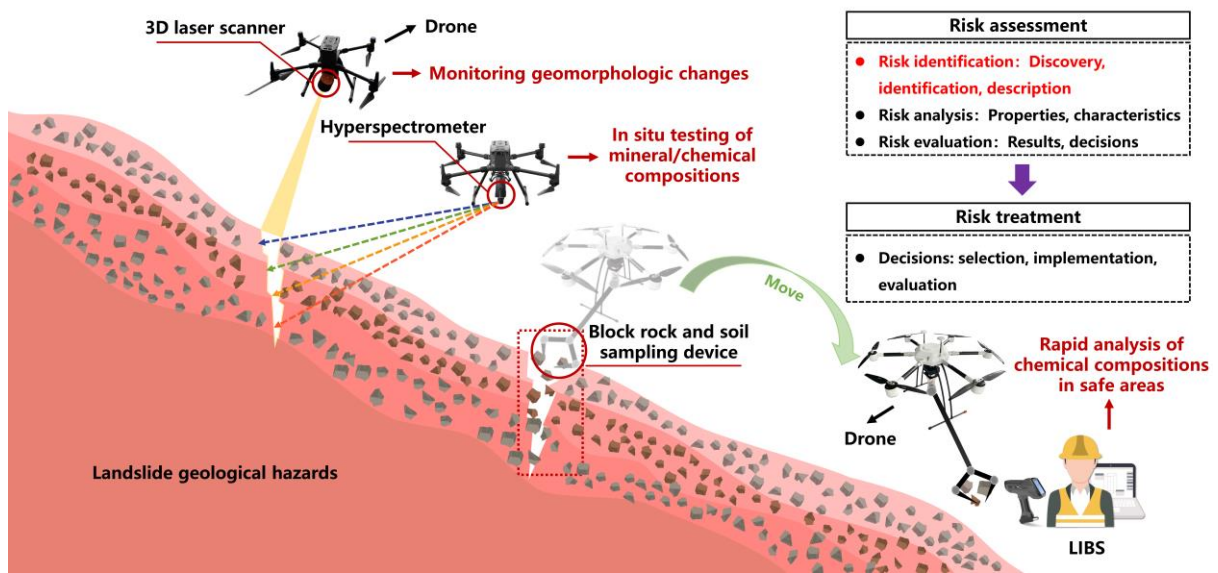
388 **Table 5.** Chemical composition combinations of 15 kinds of rocks.

No.	SiO <sub>2</sub> (%)	Al <sub>2</sub> O <sub>3</sub> (%)	TFe <sub>3</sub> O <sub>4</sub> (%)	Na <sub>2</sub> O (%)	K <sub>2</sub> O (%)	MgO (%)	CaO (%)	F1	F2	F3	F4	F5	F	Rock types
1	63.67	18.56	7.41	0.56	5.60	4.2	-	21.71	-20.06	-4.89	-0.58	4.60	1.33	Red beds
2	65.43	18.29	6.18	0.07	3.56	6.47	-	20.96	-20.88	-5.90	-0.66	2.82	0.52	
3	69.68	10.95	7.12	0.88	2.43	3.64	5.30	19.27	-19.59	-5.08	-0.52	3.66	0.50	
4	62.6	17.89	6.98	1.47	5.24	5.82	-	20.84	-19.67	-3.78	-1.14	4.21	1.21	
5	69.92	13.59	6.93	0.22	5.19	4.15	-	21.96	-20.64	-5.53	-0.54	4.13	1.12	
6	71.16	13.55	3.33	0.39	2.83	3.27	5.47	20.83	-21.96	-5.47	-2.24	0.76	-0.13	
7	68.63	15.74	1.33	1.61	4.86	2.83	5.00	21.91	-22.48	-3.47	-4.06	0.16	0.16	
8	64.53	15.67	6.75	0.30	5.35	3.6	3.80	20.31	-19.40	-4.18	-1.35	3.98	1.00	
9	69.11	15.63	4.21	0.68	5.98	4.38	-	22.76	-21.83	-4.61	-2.23	2.41	0.86	
10	66.58	11.66	7.41	1.53	4.05	8.77	-	18.94	-18.86	-3.37	-0.95	3.89	0.83	
11	73.04	11.46	1.6	1.39	3.34	2.97	6.20	21.07	-22.50	-4.15	-3.51	-0.15	-0.22	
12	70.47	12.35	6.33	1.26	5.47	1.49	2.63	22.26	-20.54	-4.62	-1.32	4.40	1.32	
13	30.36	2.35	0.15	0.33	0.28	0.70	65.84	-13.05	-6.10	16.38	-10.58	-12.25	-6.11	Limestone
14	75.27	12.73	2.22	2.47	4.59	2.67	0.06	36.73	-14.90	-12.11	-12.00	27.27	7.52	Arkose
15	78.33	18.86	1.00	0.25	1.04	0.53	-	26.62	-26.87	-10.13	-1.43	0.02	-0.20	Mudstone

389 **Note:** TFe<sub>3</sub>O<sub>4</sub> represents the content of Fe<sub>2</sub>O<sub>3</sub> and FeO. "-" represents that no content was detected. Ignoring "Fe<sub>2</sub>O<sub>3</sub>/FeO" and "MgO/CaO" without values when calculating F1-F5  
390 and F.

391 3.6 Research results application methods

392 Figure 9 shows the application methods of the research results. According to the methods for  
393 emergency management of landslide geological disasters (Fu et al., 2021), landslide risk assessment  
394 (including risk identification, risk analysis, and risk assessment) and risk management (developing and  
395 selecting treatment plans, as well as planning, implementing, and evaluating treatment methods) need  
396 to be carried out before the landslide occurs. In the field of engineering geology, risk identification is  
397 the most important prerequisite for landslide emergency response. Red beds is the slippery layer that  
398 needs to be identified in risk identification.



399

400

Figure 9. Research results used for risk identification.

401

402 At present, the commonly used risk identification method is to use drones to carry image capture  
403 devices for three-dimensional reconstruction of slope images, determine the volume of landslide  
404 accumulation, and determine the shape changes of the slope (Chen et al., 2020; Fu et al., 2021), which  
405 can be also used for mountain rescue (Wankmuller et al., 2021). Based on the drone technology,  
406 combined with the Optech Polaris LR 3D laser scanner and the HY-9070 hyperspectral analyzer of Sun  
407 Yat-sen University, the landslide shape change and remote monitoring of mineral and chemical  
408 compositions can be realized to identify whether it is a red beds landslide. It can also use a drone  
409 equipped with a block rock and soil sampling device to collect representative blocks of rock and soil  
410 within cracks to a safe area, and then use the **YL-P-3LRX Handheld Laser Induced Breakdown**

411 **Spectroscopy** for rapid analysis. Therefore, the research results can be used for rapid identification of  
412 red beds, achieving risk assessment and rapid response of geological disasters such as landslides.

413

#### 414 **4. Conclusions**

415 (1) In response to the rapid identification of red beds in geological disaster emergency response, a  
416 rapid quantitative identification criterion based on the basic chemical compositions combination rules  
417 of red beds has been established, taking into account the correlation between red beds geomorphic  
418 characteristics, mineral compositions, and chemical compositions. **It solves the current problem of**  
419 **fuzzy identification of the red beds.**

420 (2) The results indicate that the red beds in the geomorphic characteristics **have** obvious interlayer  
421 characteristics and its appearance is red. In mineral composition, the ratio of clay minerals to other  
422 minerals of red beds ranges from 0.11 to 1.50, and the content of hematite of red beds ranges from 1.5%  
423 to 10.0%. The following chemical composition combinations can be used as red beds preliminary  
424 quantification criterion:  $\text{SiO}_2+\text{Al}_2\text{O}_3 \approx 50.7\% \sim 85.0\%$ ,  $\text{Al}_2\text{O}_3/\text{SiO}_2 \approx 0.14 \sim 0.41$ ,  
425  $\text{FeO}+\text{Fe}_2\text{O}_3 \approx 0.9\% \sim 7.9\%$ ,  $\text{Fe}_2\text{O}_3/\text{FeO} \approx 1.52 \sim 7.70$ ,  $\text{K}_2\text{O}+\text{Na}_2\text{O} \approx 1.6\% \sim 6.8\%$ ,  
426  $\text{Na}_2\text{O}/\text{K}_2\text{O} \approx 0.02 \sim 0.43$ ,  $\text{CaO}+\text{MgO} \approx 0.8\% \sim 9.2\%$ . And the **principal component features** can serve  
427 as a rapid quantitative criterion for distinguishing red beds:  $F1=-3.36 \sim 23.55$ ,  $F2=-23.00 \sim 3.11$ ,  $F3=-$   
428  $10.12 \sim 4.88$ ,  $F4=-2.21 \sim 4.52$ ,  $F5=-0.97 \sim 7.30$ , and  $F=-0.67 \sim 1.89$ . **The reliability of the quantitative**  
429 **criterion was verified by collecting 15 kinds of rocks and analyzing their chemical composition**  
430 **combinations.**

431 (3) The combination of research results with existing landslide geological hazard risk identification  
432 techniques can effectively carry out rapid response to geological disasters, which is very important for  
433 emergency response to geological disasters. Moreover, the research results can also be applied to the  
434 quantitative identification of red beds in other fields such as resources, ecology, environment, energy,  
435 materials, etc.

436

#### 437 **Declarations**

438 **Availability of data and materials**

439 The data that support the findings of this study are available in supplementary materials.

440 **Competing interests**

441 The authors declare no conflict of interest. The funders had no role in the design of the study; in  
442 the collection, analyses, or interpretation of data; in the writing of the manuscript, or in the decision to  
443 publish the results.

444 **Funding**

445 The research is supported by the National Natural Science Foundation of China (NSFC) (Grant  
446 Numbers: 42293354, 42293351, 42293355, 42277131, 41977230, and 42293350).

447 **Authors' contributions**

448 Conceptualization, C.Z. and Z.L.; methodology, G.C. and Z.L.; software, G.C. and L.K.; validation,  
449 G.C., L.K., and Z.L.; formal analysis, C.Z. and Z.L.; investigation, G.C., J.L., and L.Y.; resources, G.C.  
450 and L.K.; data curation, G.C., J.L., L.Y. and L.K.; writing—original draft preparation, G.C. and L.K.;  
451 writing—review and editing, G.C., Z.L., and L.Z.; visualization, L.Y.; supervision, Z.L. and L.Z.;  
452 project administration, C.Z.; funding acquisition, C.Z. All authors have read and agreed to the published  
453 version of the manuscript.

454 **Acknowledgments**

455 The authors would like to thank the anonymous reviewers for their very constructive and helpful  
456 comments.

457 **Supplementary Materials**

458 Supplementary Table 1: Mineral compositions of the red beds.

459 Supplementary Table 2: Chemical compositions of the red beds.

460 Supplementary Table 3: Chemical compositions of the andesite.

461 Supplementary Table 4: Chemical compositions of the basalt.

462 Supplementary Table 5: Chemical compositions of the diorite.

463 Supplementary Table 6: Chemical compositions of the granite.

464 Supplementary Table 7: Chemical compositions of the gneiss.

465 Supplementary Table 8: Chemical compositions of the marble.



466 Supplementary Table 9: Chemical compositions of the arkose.  
467 Supplementary Table 10: Chemical compositions of the black-shale.  
468 Supplementary Table 11: Chemical compositions of the breccia.  
469 Supplementary Table 12: Chemical compositions of the claystone.  
470 Supplementary Table 13: Chemical compositions of the dolomite.  
471 Supplementary Table 14: Chemical compositions of the lignite.  
472 Supplementary Table 15: Chemical compositions of the limestone.  
473 Supplementary Table 16: Chemical compositions of the marl.  
474 Supplementary Table 17: Chemical compositions of the mudstone.  
475 Supplementary Table 18: Chemical compositions of the siliciclastic.  
476 Supplementary Table 19: Chemical compositions of the tuff.

477

## 478 **References**

- 479 Anbarasu, K., Sengupta, A., Gupta, S., and Sharma, S. P.: Mechanism of activation of the Lanta Khola landslide  
480 in Sikkim Himalayas, *Landslides*, 7, 135-147, 10.1007/s10346-009-0193-0, 2010.
- 481 Bai, Y., Shan, R., Ju, Y., Wu, Y., Tong, X., Han, T., and Dou, H.: Experimental study on the strength, deformation  
482 and crack evolution behaviour of red sandstone samples containing two ice-filled fissures under triaxial  
483 compression, *Cold Regions Science and Technology*, 174, 10.1016/j.coldregions.2020.103061, 2020.
- 484 Bankole, O. M., Albani, A. E., Meunier, A., Rouxel, O. J., Oisgauthier-Lafaye, F., and Bekker, A.: Origin of Red  
485 Beds in the Paleoproterozoic Franceville Basin, Gabon, and Implications for Sandstone-Hosted Uranium  
486 Mineralization, *Am J Sci*, 316, 839-872, 10.2475/09.2016.02, 2016.
- 487 Chen, J., Dai, F., Xu, L., Chen, S., Wang, P., Long, W., and Shen, N.: Properties and microstructure of a natural  
488 slip zone in loose deposits of red beds, southwestern China, *Eng Geol*, 183, 53-64,  
489 10.1016/j.enggeo.2014.10.004, 2014.
- 490 Chen, L. F., Tian, X. K., Xia, D. S., Nie, Y. L., Lu, L. Q., Yang, C., and Zhou, Z. X.: Novel Colorimetric Method  
491 for Simultaneous Detection and Identification of Multimetal Ions in Water: Sensitivity, Selectivity, and  
492 Recognition Mechanism, *Acs Omega*, 4, 5915-5922, 10.1021/acsomega.9b00312, 2019.
- 493 Chen, S. J., Xiang, C. C., Kang, Q., Zhong, W., Zhou, Y. L., and Liu, K.: Accurate landslide detection leveraging  
494 UAV-based aerial remote sensing, *Iet Commun*, 14, 2434-2441, 10.1049/iet-com.2019.1115, 2020.

495 Chen, Z. Y., Männik, P., Fan, J. X., Wang, C. Y., Chen, Q., Sun, Z. Y., Chen, D. Y., and Li, C.: Age of the Silurian  
496 Lower Red Beds in South China: Stratigraphical Evidence from the Sanbaiti Section, *J Earth Sci-China*, 32,  
497 524-533, [10.1007/s12583-020-1350-6](https://doi.org/10.1007/s12583-020-1350-6), 2021.

498 Ciftci, E., Hogan, J. P., Kolayli, H., and Cadirli, E.: Natrolite, an unusual rock - Occurrence and petrographic  
499 and geochemical characteristics (eastern Turkey), *Clay Clay Miner*, 56, 207-221,  
500 [10.1346/Ccmn.2008.0560206](https://doi.org/10.1346/Ccmn.2008.0560206), 2008.

501 Contino, A., Bova, P., Esposito, G., Giuffrè, I., and Monteleone, S.: Historical analysis of rainfall-triggered  
502 rockfalls: the case study of the disaster of the ancient hydrothermal Sclafani Spa (Madonie Mts, northern-  
503 central Sicily, Italy) in 1851, *Nat Hazard Earth Sys*, 17, 2229-2243, [10.5194/nhess-17-2229-2017](https://doi.org/10.5194/nhess-17-2229-2017), 2017.

504 Cui, G., Zhou, C., Liu, Z., Xia, C., and Zhang, L.: The synthesis of soft rocks based on physical and mechanical  
505 properties of red mudstone, *International Journal of Rock Mechanics and Mining Sciences*, 151, 105037,  
506 <https://doi.org/10.1016/j.ijrmms.2022.105037>, 2022.

507 Cunha, P., Marques, J., Curi, N., Pereira, G. T., and Lepsch, I. F.: Geomorphic surfaces and latosol (oxisol)  
508 characteristics on a sandstone/basalt sequence from the Jaboticabal region, Sao Paulo State, Brazil, *Rev Bras*  
509 *Cienc Solo*, 29, 81-90, [Doi 10.1590/S0100-06832005000100009](https://doi.org/10.1590/S0100-06832005000100009), 2005.

510 de Montety, V., Marc, V., Emblanch, C., Malet, J. P., Bertrand, C., Maquaire, O., and Bogaard, T. A.: Identifying  
511 the origin of groundwater and flow processes in complex landslides affecting black marls: insights from a  
512 hydrochemical survey, *Earth Surf Proc Land*, 32, 32-48, [10.1002/esp.1370](https://doi.org/10.1002/esp.1370), 2007.

513 Feizizadeh, B., Garajeh, M. K., Blaschke, T., and Lakes, T.: An object based image analysis applied for volcanic  
514 and glacial landforms mapping in Sahand Mountain, Iran, *Catena*, 198, ARTN 105073  
515 [10.1016/j.catena.2020.105073](https://doi.org/10.1016/j.catena.2020.105073), 2021.

516 Fu, L., Zhu, J., Li, W.-l., You, J.-g., and Hua, Z.-y.: Fast estimation method of volumes of landslide deposit by  
517 the 3D reconstruction of smartphone images, *Landslides*, 18, 3269-3278, [10.1007/s10346-021-01702-9](https://doi.org/10.1007/s10346-021-01702-9),  
518 2021.

519 Gao, F., Wu, X., and Deng, R.: The distribution of red beds and analysis on engineering characteristics of  
520 mudstone in Guangxi, *Journal of Geological Hazards and Environment Preservation*, 28, 48-52, 2017.

521 Garajeh, M. K., Feizizadeh, B., Blaschke, T., and Lakes, T.: Detecting and mapping karst landforms using object-  
522 based image analysis: Case study: Takht-Soleiman and Parava Mountains, Iran, *The Egyptian Journal of*  
523 *Remote Sensing and Space Science*, 25, 473-489, <https://doi.org/10.1016/j.ejrs.2022.03.009>, 2022.

524 Gokbulak, F. and Ozcan, M.: Hydro-physical properties of soils developed from different parent materials,  
525 Geoderma, 145, 376-380, 10.1016/j.geoderma.2008.04.006, 2008.

526 Hale, S., Ries, X., Jaeggi, D., and Blum, P.: Mechanical and hydraulic properties of the excavation damaged zone  
527 (EDZ) in the Opalinus Clay of the Mont Terri rock laboratory, Switzerland, Solid Earth, 12, 1581-1600,  
528 10.5194/se-12-1581-2021, 2021.

529 Han, P. H., Zhang, C., Wang, X. J., and Wang, L.: Study of mechanical characteristics and damage mechanism  
530 of sandstone under long-term immersion, Eng Geol, 315, ARTN 107020  
531 10.1016/j.enggeo.2023.107020, 2023.

532 Harp, E. L., Dart, R. L., and Reichenbach, P.: Rock fall simulation at Timpanogos Cave National Monument,  
533 American Fork Canyon, Utah, USA, Landslides, 8, 373-379, 10.1007/s10346-010-0251-7, 2011.

534 He, J., Niu, F., Luo, F., Jiang, H., He, P., and Ju, X.: Mechanical properties and modified binary-medium  
535 constitutive model for red-bed soft rock subjected to freeze-thaw cycles, Cold Reg Sci Technol, 209,  
536 10.1016/j.coldregions.2023.103803, 2023.

537 He, K., Ma, G. T., and Hu, X. W.: Formation mechanisms and evolution model of the tectonic-related ancient  
538 giant basalt landslide in Yanyuan County, China, Nat Hazards, 106, 2575-2597, 10.1007/s11069-021-04555-  
539 6, 2021.

540 Hong, H., Li, Z., and Xiao, P.: Clay Mineralogy Along the Laterite Profile in Hubei, South China: Mineral  
541 Evolution and Evidence for Eolian Origin, Clay Clay Miner, 57, 602-615, 10.1346/Ccmn.2009.0570508,  
542 2009.

543 Hu, X., Wang, C., Li, X., and Luba, J.: Upper Cretaceous oceanic red beds in southern Tibet: Lithofacies,  
544 environments and colour origin, Sci China Ser D, 49, 785-795, 10.1007/s11430-006-0785-7, 2006.

545 Jian, W. X., Wang, Z. J., and Yin, K. L.: Mechanism of the Anlesi landslide in the Three Gorges Reservoir, China,  
546 Eng Geol, 108, 86-95, 10.1016/j.enggeo.2009.06.017, 2009.

547 Jiang, H., Xia, Y., Li, J., Liu, S., Zhang, M., and Wang, Y.: Controlling the Iron Migration Mechanism for the  
548 Cretaceous Sediment Color Variations in Sichuan Basin, China, Acs Omega, 7, 480-495,  
549 10.1021/acsomega.1c04893, 2022.

550 Kavvasdas, M., Roumpos, C., and Schilizzi, P.: Stability of Deep Excavation Slopes in Continuous Surface Lignite  
551 Mining Systems, Geotechnical and Geological Engineering, 38, 791-812, 10.1007/s10706-019-01066-x,  
552 2020.

553 Kirsch, M., Lorenz, S., Zimmermann, R., Tusa, L., Mockel, R., Hodl, P., Booyesen, R., Khodadadzadeh, M., and  
554 Gloaguen, R.: Integration of Terrestrial and Drone-Borne Hyperspectral and Photogrammetric Sensing  
555 Methods for Exploration Mapping and Mining Monitoring, *Remote Sens-Basel*, 10, 10.3390/rs10091366,  
556 2018.

557 Kong, L. W., Zeng, Z. X., Bai, W., and Wang, M.: Engineering geological properties of weathered swelling  
558 mudstones and their effects on the landslides occurrence in the Yanji section of the Jilin-Hunchun high-speed  
559 railway, *B Eng Geol Environ*, 77, 1491-1503, 10.1007/s10064-017-1096-2, 2018.

560 Li, A., Deng, H., Zhang, H., Liu, H., and Jiang, M.: The shear-creep behavior of the weak interlayer mudstone in  
561 a red-bed soft rock in acidic environments and its modeling with an improved Burgers model, *Mech Time-  
562 Depend Mat*, 27, 1-18, 10.1007/s11043-021-09523-y, 2023.

563 Li, J., Xu, Q., Hu, Z., Liu, H., Zhang, Q., Lu, Y., and Wang, S.: Experimental research on softening of undisturbed  
564 saturated slip soil in eastern of Sichuan province red bed, *Chinese Journal of Rock Mechanics and  
565 Engineering*, 34, 4333-4342, 2015.

566 Li, S., Chen, J., and Yi, G.: Experimental study on the relationship between micro-characteristics and compressive  
567 strength of the red bed rock, *Geotechnical Investigation and Surveying*, 41, 1-5, 2013.

568 Li, X. N., Zhu, B. L., and Wu, X. Y.: Swelling characteristics of soils derived from black shales heightened by  
569 cations in Northern Chongqing, China, *J Mt Sci-Engl*, 13, 1107-1119, 10.1007/s11629-015-3576-9, 2016.

570 Liu, C., He, C., and He, M.: Engineering geology study on failure of red beds slopes along railway in the west of  
571 Hunan Province, *The Chinese Journal of Geological Hazard and Control*, 18, 58-62, 2007.

572 Liu, J., Wei, J. H., Hu, H., Wu, J. M., Sun, S. R., and Kanungo, D. P.: Research on the engineering geological  
573 conditions and stability evaluation of the B2 talus slide at the Jin'an Bridge hydropower station, China, *B  
574 Eng Geol Environ*, 77, 105-125, 10.1007/s10064-017-1005-8, 2018.

575 Liu, J., Xu, Q., Wang, S., Siva Subramanian, S., Wang, L., and Qi, X.: Formation and chemo-mechanical  
576 characteristics of weak clay interlayers between alternative mudstone and sandstone sequence of gently  
577 inclined landslides in Nanjiang, SW China, *B Eng Geol Environ*, 79, 4701-4715, 10.1007/s10064-020-  
578 01859-y, 2020.

579 Liu, X., Zhao, M., Su, Y., and Long, Y.: Grey Correlation Analysis of Slake Durability of Red Bed Weak Rock,  
580 *Journal of Hunan University (Natural Sciences)*, 33, 16-20, 2006.

581 Marat, A. R., Tamas, T., Samsudean, C., and Gheorghiu, R.: Physico-Mechanical and Mineralogical  
582 Investigations of Red Bed Slopes (Cluj-Napoca, Romania), *B Eng Geol Environ*, 81, 10.1007/s10064-021-  
583 02542-6, 2022.

584 Migon, P., Woo, K. S., and Kasprzak, M.: Landform Recognition in Granite Mountains in East Asia (Seoraksan,  
585 Republic of Korea, and Huangshan and Sanqingshan, China) - a Contribution of Geomorphology to the  
586 Unesco World Heritage, *Quaest Geogr*, 37, 103-114, 10.2478/quageo-2018-0008, 2018.

587 Moonjun, R., Shrestha, D. P., Jetten, V. G., and van Ruitenbeek, F. J. A.: Application of airborne gamma-ray  
588 imagery to assist soil survey: A case study from Thailand, *Geoderma*, 289, 196-212,  
589 10.1016/j.geoderma.2016.10.035, 2017.

590 Nance, H. S.: Interfingering of evaporites and red beds: an example from the queen/grayburg formation, Texas,  
591 *Sediment Geol*, 56, 357-381, 2015.

592 Ni, L. T., Zhong, J. H., Shao, Z. F., Li, Y., Mao, C., and Liu, S. X.: Characteristics, Genesis, and Sedimentary  
593 Environment of Duplex-Like Structures in the Jurassic Sediments of Western Qaidam Basin, China, *J Earth  
594 Sci-China*, 26, 677-689, 10.1007/s12583-015-0578-2, 2015.

595 Perez-Rey, I., Riquelme, A., Gonzalez-deSantos, L. M., Estevez-Ventosa, X., Tomas, R., and Alejano, L. R.: A  
596 multi-approach rockfall hazard assessment on a weathered granite natural rock slope, *Landslides*, 16, 2005-  
597 2015, 10.1007/s10346-019-01208-5, 2019.

598 Perri, F., Critelli, S., Martín-Algarra, A., Martín-Martín, M., Perrone, V., Mongelli, G., and Zattin, M.: Triassic  
599 redbeds in the Malaguide Complex (Betic Cordillera - Spain): Petrography, geochemistry and geodynamic  
600 implications, *Earth-Sci. Rev.*, 117, 1-28, 10.1016/j.earscirev.2012.11.002, 2013.

601 Qiao, L. P., Wang, Z. C., and Huang, A. D.: Alteration of Mesoscopic Properties and Mechanical Behavior of  
602 Sandstone Due to Hydro-Physical and Hydro-Chemical Effects, *Rock Mechanics and Rock Engineering*, 50,  
603 255-267, 10.1007/s00603-016-1111-0, 2017.

604 Rainoldi, A. L., Franchini, M., Beaufort, D., Mozley, P., Giusiano, A., Nora, C., Patrier, P., Impiccini, A., and  
605 Pons, J.: Mineral reactions associated with hydrocarbon paleomigration in the Huincul High, Neuquen Basin,  
606 Argentina, *Geol Soc Am Bull*, 127, 1711-1729, 10.1130/B31201.1, 2015.

607 San, N. E., Topal, T., and Akin, M. K.: Rockfall Hazard Assessment Around Ankara Citadel (Turkey) Using  
608 Rockfall Analyses and Hazard Rating System, *Geotechnical and Geological Engineering*, 38, 3831-3851,  
609 10.1007/s10706-020-01261-1, 2020.

610 Triantafyllou, A., Mattielli, N., Clerbois, S., Da Silva, A. C., Kaskes, P., Claeys, P., Devleeschouwer, X., and  
611 Brkojewitsch, G.: Optimizing multiple non-invasive techniques (PXRF, pMS, IA) to characterize coarse-  
612 grained igneous rocks used as building stones, *J Archaeol Sci*, 129, 10.1016/j.jas.2021.105376, 2021.

613 Uchida, E., Ogawa, Y., Maeda, N., and Nakagawa, T.: Deterioration of stone materials in the Angkor monuments,  
614 Cambodia, *Eng Geol*, 55, 101-112, Doi 10.1016/S0013-7952(99)00110-6, 2000.

615 Underwood, S. J., Schultz, M. D., Berti, M., Gregoretti, C., Simoni, A., Mote, T. L., and Saylor, A. M.:  
616 Atmospheric circulation patterns, cloud-to-ground lightning, and locally intense convective rainfall  
617 associated with debris flow initiation in the Dolomite Alps of northeastern Italy, *Nat Hazard Earth Sys*, 16,  
618 509-528, 10.5194/nhess-16-509-2016, 2016.

619 Wang, D., Li, X.-b., Peng, K., Ma, C., Zhang, Z., and Liu, X.: Geotechnical characterization of red shale and its  
620 indication for ground control in deep underground mining, *J Cent South Univ*, 25, 2979-2991,  
621 10.1007/s11771-018-3968-4, 2018.

622 Wang, F. W., Chen, Y., Peng, X. L., Zhu, G. L., Yan, K. M., and Ye, Z. H.: The fault-controlled Chengtian  
623 landslide triggered by rainfall on 20 May 2021 in Songyang County, Zhejiang Province, China, *Landslides*,  
624 19, 1751-1765, 10.1007/s10346-022-01891-x, 2022a.

625 Wang, L., Wang, L., Zhang, W., Meng, X., Liu, S., and Zhu, C.: Time series prediction of reservoir bank landslide  
626 failure probability considering the spatial variability of soil properties, *J Rock Mech Geotech*,  
627 <https://doi.org/10.1016/j.jrmge.2023.11.040>, 2024.

628 Wang, M., Qi, Y. A., Li, D., Dai, M. Y., and Chang, Y. G.: Ichnofabrics and Their Environmental Interpretation  
629 from the Fluvial Deposits of the Middle Triassic Youfangzhuang Formation in Western Henan, Central China,  
630 *J Earth Sci-China*, 25, 648-661, 10.1007/s12583-014-0454-2, 2014.

631 Wang, Y., Liu, J., Yan, S., Yu, L., and Yin, K.: Estimation of probability distribution of shear strength of slip  
632 zone soils in Middle Jurassic red beds in Wanzhou of China, *Landslides*, 14, 2165-2174, 10.1007/s10346-  
633 017-0890-z, 2017.

634 Wang, Y., Tang, H., Huang, J., Wen, T., Ma, J., and Zhang, J.: A comparative study of different machine learning  
635 methods for reservoir landslide displacement prediction, *Eng Geol*, 298, 106544,  
636 <https://doi.org/10.1016/j.enggeo.2022.106544>, 2022b.

637 Wankmuller, C., Kunovjanek, M., and Mayrgundter, S.: Drones in emergency response-evidence from cross-  
638 border, multi-disciplinary usability tests, *Int J Disast Risk Re*, 65, 10.1016/j.ijdr.2021.102567, 2021.

639 Wild, K. M., Walter, P., and Amann, F.: The response of Opalinus Clay when exposed to cyclic relative humidity  
640 variations, *Solid Earth*, 8, 351-360, 10.5194/se-8-351-2017, 2017.

641 Wu, L. Z., Zhang, L. M., Zhou, Y., Xu, Q., Yu, B., Liu, G. G., and Bai, L. Y.: Theoretical analysis and model test  
642 for rainfall-induced shallow landslides in the red-bed area of Sichuan, *Bulletin of Engineering Geology and  
643 the Environment*, 77, 1343-1353, 10.1007/s10064-017-1126-0, 2018.

644 Xia, K. Z., Chen, C. X., Zheng, Y., Zhang, H. N., Liu, X. M., Deng, Y. Y., and Yang, K. Y.: Engineering geology  
645 and ground collapse mechanism in the Chengchao Iron-ore Mine in China, *Eng Geol*, 249, 129-147,  
646 10.1016/j.enggeo.2018.12.028, 2019.

647 Xue, Y., Wang, Q., Ma, L., Yu, Y., and Zhang, R.: Mechanisms and controlling factors of heave in summer for  
648 high-speed railway cutting: A case study of Northwest China, *Construction and Building Materials*, 365,  
649 10.1016/j.conbuildmat.2022.130061, 2023.

650 Yan, L. B., Peng, H., Zhang, S. Y., Zhang, R. X., Kasanin-Grubin, M., Lin, K. R., and Tu, X. J.: The Spatial  
651 Patterns of Red Beds and Danxia Landforms: Implication for the formation factors-China, *Sci Rep-Uk*, 9,  
652 10.1038/s41598-018-37238-7, 2019.

653 Yang, Y., Zhou, J., Xu, F., and Xing, H.: An Experimental Study on the Water-Induced Strength Reduction in  
654 Zigong Argillaceous Siltstone with Different Degree of Weathering, *Adv Mater Sci Eng*,  
655 10.1155/2016/4956986, 2016.

656 Yao, H., Jia, S., Gan, W., Zhang, Z., and Lu, K.: Properties of Crushed Red-Bed Soft Rock Mixtures Used in  
657 Subgrade, *Adv Mater Sci Eng*, 2016, 10.1155/2016/9624974, 2016.

658 Zha, F., Huang, K., Kang, B., Sun, X., Su, J., Li, Y., and Lu, Z.: Deterioration Characteristic and Constitutive  
659 Model of Red-Bed Argillaceous Siltstone Subjected to Drying-Wetting Cycles, *Lithosphere-Uk*, 2022,  
660 8786210, 10.2113/2022/8786210, 2022.

661 Zhang, M., Yin, Y., and Huang, B.: Mechanisms of rainfall-induced landslides in gently inclined red beds in the  
662 eastern Sichuan Basin, SW China, *Landslides*, 12, 973-983, 10.1007/s10346-015-0611-4, 2015.

663 Zhang, S., Xu, Q., and Hu, Z. M.: Effects of rainwater softening on red mudstone of deep-seated landslide,  
664 Southwest China, *Eng Geol*, 204, 1-13, 10.1016/j.enggeo.2016.01.013, 2016.

665 Zhang, W., Lin, S., Wang, L., Wang, L., Jiang, X., and Wang, S.: A novel creep contact model for rock and its  
666 implement in discrete element simulation, *Comput Geotech*, 167, 106054,  
667 <https://doi.org/10.1016/j.compgeo.2023.106054>, 2024.

668 Zhang, Y., Li, F., and Chen, J.: Analysis of the interaction between mudstone and water, *Journal of Engineering*  
669 *Geology*, 16, 22-26, 2008.

670 Zhang, Z., Gao, W., Zeng, C., Tang, X., and Wu, J.: Evolution of the disintegration breakage of red-bed soft rock  
671 using a logistic regression model, *Transp Geotech*, 24, 10.1016/j.trgeo.2020.100382, 2020.

672 Zhang, Z. H., Chen, X. C., Yao, H. Y., Huang, X., and Chen, L. W.: Experimental Investigation on Tensile  
673 Strength of Jurassic Red-Bed Sandstone under the Conditions of Water Pressures and Wet-Dry Cycles, *Ksce*  
674 *J Civ Eng*, 25, 2713-2724, 10.1007/s12205-021-1404-z, 2021.

675 Zhang, Z. L., Wang, T., Wu, S. R., Tang, H. M., and Liang, C. Y.: The role of seismic triggering in a deep-seated  
676 mudstone landslide, China: Historical reconstruction and mechanism analysis, *Eng Geol*, 226, 122-135,  
677 10.1016/j.enggeo.2017.06.001, 2017.

678 Zhao, M., Liu, X., and Su, Y.: Experimental studies on engineering properties of red bed material containing  
679 slaking rock, *Chinese Journal of Geotechnical Engineering*, 27, 667-671, 2005.

680 Zhou, C., Hu, Y., Xiao, T., Ou, Q., and Wang, L.: Analytical model for reinforcement effect and load transfer of  
681 pre-stressed anchor cable with bore deviation, *Construction and Building Materials*, 379, 131219,  
682 <https://doi.org/10.1016/j.conbuildmat.2023.131219>, 2023a.

683 Zhou, C., Yu, L., Huang, Z., Liu, Z., and Zhang, L.: Analysis of microstructure and spatially dependent  
684 permeability of soft soil during consolidation deformation, *Soils Found*, 61, 708-733,  
685 <https://doi.org/10.1016/j.sandf.2021.02.004>, 2021.

686 Zhou, C., Liu, Z., Xue, Y., Li, Y., Fan, X., Chen, W., and Sun, P.: Some thoughts on basic research of red beds  
687 disaste, *Journal of Engineering Geology*, 31, 689-705, 10.13544/j.cnki.jeg.2022-0842, 2023b.

688 Zhu, B., Hu, H., and Chen, Q.: Preliminary study on the characteristics and hazards of M - shaped roadcut slope  
689 in red beds, *Journal of Engineering Geology*, 11, 411-415, 2003.

690